Journal Pre-proof

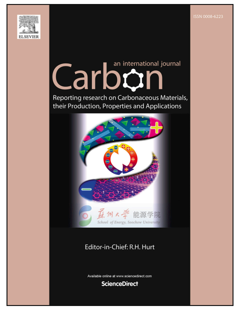

Chem-mechanical polishing influenced morphology, spectral and electrochemical characteristics of boron doped diamond

M. Zelenský, J. Fischer, S. Baluchová, L. Klimša, J. Kopeček, M. Vondráček, L. Fekete, J. Eidenschink, F.-M. Matysik, S. Mandal, O.A. Williams, M. Hromadová, V. Mortet, K. Schwarzová-Pecková, A. Taylor

PII: S0008-6223(22)00991-5

DOI: https://doi.org/10.1016/j.carbon.2022.11.069

Reference: CARBON 17709

To appear in: *Carbon*

Received Date: 30 June 2022

Revised Date: 11 November 2022

Accepted Date: 22 November 2022

Michal Zelenský: Writing- Original draft preparation, Investigation, Visualization. **Jan Fischer:** Methodology**,** Funding acquisition. **Simona Baluchová** Investigation, Visualization. **Ladislav Klimša:** Investigation, Visualization. **Jaromir Kopeček:** Investigation. **Martin Vondráček:** Investigation, Visualization. **Ladislav Fekete:** Investigation, Visualization. **Johannes Eidenschink** Investigation, Visualization. **Frank-Michael Matysik** Investigation, Supervision. **Soumen Mandal:** Investigation **Oliver Williams:** Investigation. **Vincent Mortet:** Conceptualization. **Karolina Schwarzová-Pecková:** Writing - Review & Editing, Conceptualization, Supervision. **Andrew Taylor:** Writing - Review & Editing, Investigation, Funding acquisition.

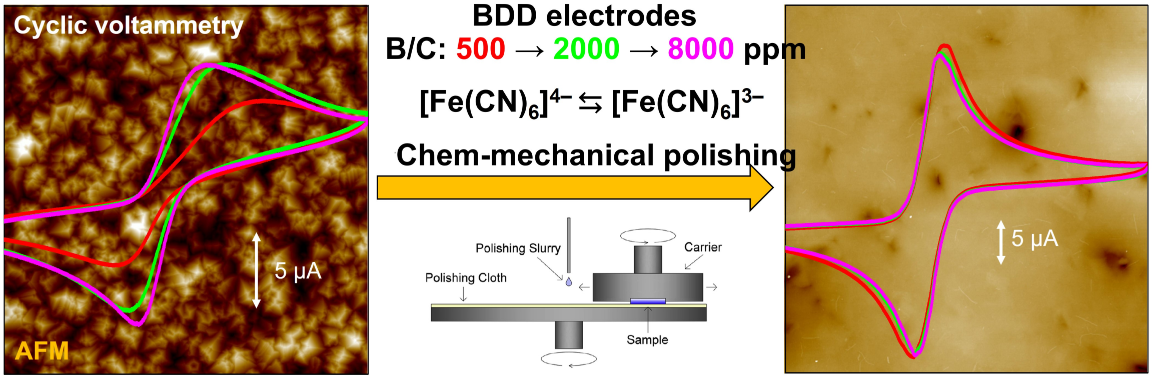
Cyclic voltammetry
AFM
5 μA
BDD electrodes
B/C: 500 → 2000 → 8000 ppm
[Fe(CN)6]4– ⇆ [Fe(CN)6]3–
Chem-mechanical polishing
Polishing Slurry
Carrier
Polishing Cloth
Sample
5 μA

Chem-mechanical polishing influenced morphology, spectral and electrochemical characteristics of boron doped diamond

Zelenský M[1], Fischer J[1], Baluchová S[1], Klimša L[2], Kopeček J[2], Vondráček M[2], Fekete L[2], Eidenschink J[3], Matysik F-M[3], Mandal S[4], Williams OA[4], Hromadová M[5], Mortet V[2], Schwarzová-Pecková K[1], Taylor A[2*]

[1]Charles University, Faculty of Science, Department of Analytical Chemistry, UNESCO Laboratory of Environmental Electrochemistry, Albertov 2038/6, 128 00 Prague 2, Czech Republic

[2]FZU – Institute of Physics of the Czech Academy of Sciences, Na Slovance 1999/2, 182 21 Prague 8, Czech Republic

[3]University of Regensburg, Institute of Analytical Chemistry, Chemo- and Biosensors, Universitätsstraße 31, 93053 Regensburg, Germany

[4]Cardiff University, School of Physics and Astronomy, Queen's Buildings North Building, 5 The Parade, Newport Road, CF24 3AA Cardiff, United Kingdom

[5]J. Heyrovský Institute of Physical Chemistry of the CAS, Dolejškova 2155/3, 182 23 Prague 8, Czech Republic

Abstract

In this study complex characterization and comparison of as-grown and chemical-mechanical (CM) polished ultra-thin (≤ 500 nm) boron doped diamond (BDD) electrodes with various boron content (0.58 to 4.4 × 10^{21} cm^{-3}, deposited with B/C 500 – 8000 ppm) was performed. Atomic force and scanning electron microscopy were used to compare morphological changes and confirm the reduction in roughness down to ≤ 2 nm. High-quality CM polishing enabled electron backscatter diffraction leading for evaluation of grain size distribution (mean 0.3 µm) and preferred grain texture, {011}. X-ray photoelectron spectroscopy confirmed an increase in the B content on the surface of CM polished electrodes as result of exposure of boron atoms incorporated into the bulk for highly doped BDD_{4000} and BDD_{8000} electrodes. Additionally, CM polished BDD electrodes are shown to possess uniform distribution of conductivity as proved by scanning electrochemical microscopy. This was reflected in faster heterogenous electron transfer kinetics for inner-sphere redox markers ($[Fe(CN)_6]^{3-/4-}$ and dopamine) and higher values of double layer capacitance in comparison with as-grown electrodes. These changes were more pronounced for low doped electrodes. Finally, the improvement in electrochemical characteristics was demonstrated by superior electroanalytical performance of CM polished BDD electrodes for dopamine detection.

*Andrew Taylor. Tel: +420 266 052 634 E-mail: taylor@fzu.cz

1. Introduction

Boron doped diamond (BDD) electrodes, with sp^3 hybridized carbon, are a very perspective electrode material thanks to properties of diamond such as chemical inertness and hardness. The low capacitance of BDD layers leads to low and stable background currents, and thanks to the high overpotential of hydrogen and oxygen evolution reactions, they provide a wide potential window, particularly at positive potentials in aqueous media. All these properties make BDD electrodes a very useful material for electroanalytical applications [1–4]. Nevertheless, the electrochemical properties of BDD electrodes are highly influenced by many factors, *e.g.*, boron doping level, sp^2 carbon impurities, crystal orientation, grain boundaries, and surface termination (H-, or O-terminated surface) created by pre-treatment of BDD surfaces. Each of these factors play a significant role in influencing heterogenous electron transfer (HET) kinetics, in particular for inner-sphere redox processes [5–9].

Boron concentration influences the conductivity of BDD layers, where the theoretical value for semiconductive/metallic-like conductivity transition is 2×10^{20} boron atoms cm^{-3} [10–13]. The boron dopant level is also related to the sp^2 carbon content in BDD layers, as with higher B/C ratio in the gas phase during chemical vapour deposition (CVD), crystalline quality diminishes and BDD layers possess higher grain boundary content. An increased sp^2 carbon/boron content increases the number of charger carriers in BDD layers, which results in an increase in background current and therefore shortens potential window [11,14–16]. Further, it leads to acceleration of HET kinetics for inner-sphere redox systems [6,17–19]. However, unwanted adsorption of reaction (by)products can occur due to higher sp^2 carbon content in highly doped BDD layers, which can cause surface fouling [20].

Surface termination is another crucial factor determining electrochemical properties of BDD layers. It can be easily varied by in-situ electrochemical pre-treatment of the surface. Cathodic pre-treatment in the potential region of hydrogen evolution leads to hydrophobic H-terminated surfaces possessing limited surface conductivity, while anodic pre-treatment in the region of water decomposition to hydroxyl radicals leads to O-termination [21,22]. These surfaces, containing -C−OH, -C=O, -C−O−C- and -COOH groups, are partially negatively charged, thus hydrophilic and their surface conductivity is minimal [2,23]. Further, they exhibit slow HET kinetics for inner-sphere redox markers due to the presence of π-electrons in oxygen functional groups [24]. Another way to treat BDD surfaces is alumina polishing, which is commonly used on other solid electrodes. This procedure presumably leads to removal of sp^2 hybridized carbon possessing oxygen functionalities, thus alumina-polished layers have a lower content of oxygen functionalities as confirmed by X-ray photoelectron spectroscopy (XPS) [12]. This polishing process was, for a long time, considered as a process that could damage a surface and create defects which can trap charge carriers, however an increasing number of analytical studies on polished surfaces confirm its stability, sufficient signal reproducibility and sensitivity thanks to fast HET kinetics [6,25–27].

While alumina-polishing only affects the sp^2 hybridized carbon and the attached oxygen functionalities, it does not change the surface morphology. Chemical-mechanical (CM) polishing, which is capable of smoothing the diamond crystallites, has been used for polishing of ultra-thin (≤ 500 nm) polycrystalline [28] and single crystal [29] undoped diamond. Here, an alkaline colloidal silica is used as a polishing fluid on a polyurethane/polyester pad. Quantum chemical simulations, on {110} surfaces, proved that strong C−O and C−Si bonds can be formed between silica and carbon atoms, which chemically activates C−C bonds between terminating carbon zigzag chains and bulk diamond. As a consequence, C−C bonds are broken, and carbon atoms can be extracted from the diamond lattice [30], leading to a final RMS surface roughness of < 2nm over large areas.

While CM polishing has been used on ultra-thin BDD layers in the past [31,32] for testing superconducting properties of BDD, or for thin (*ca* 2 μm) layers of highly doped BDD [9], the surface properties of BDD layers differing in boron content before and after polishing has not been investigated in detail. In this work a complex morphologic, spectral, and electrochemical characterization was performed to assess the effect of CM polishing in comparison with polycrystalline as-grown BDD electrodes deposited at B/C ratios of 500, 1000, 2000, 4000, 8000 ppm in the gas phase during chemical vapour deposition (CVD). A wide range of techniques including Raman spectroscopy, scanning electron (SEM) and atomic force microscopy (AFM), XPS, scanning electrochemical microscopy (SECM), electron backscatter diffraction (EBSD), electrochemical impedance spectroscopy (EIS), square wave voltammetry (SWV) and cyclic voltammetry (CV) for evaluation of heterogenous electrons transfer (HET) kinetics of outer- and inner-sphere redox markers was used to assess the performance of CM polished BDD electrodes and to contribute to understanding of the interplay between the boron and sp^2 carbon content, oxygen content and morphology and physical and electrochemical properties of BDD.

2. Experimental

2.1. Synthesis of polycrystalline BDD layers

Polycrystalline BDD layers were deposited on 2-inch conductive Si wafers using a 1.5 kW resonance cavity microwave plasma enhanced CVD system (AX5010 from Seki Diamond Systems) using well established growth conditions, *i.e.*, 0.5% CH_4 in H_2, gas pressure = 50 mbar, microwave power = 1150 W, substrate temperature ca 750 °C and a growth duration of 5 h to produce layers with thicknesses ≤ 500 nm. Boron doping was obtained by the addition of trimethylboron in the gas phase to give a B/C ratio ranging from 500 to 8000 ppm (BDD_{500} – BDD_{8000}). Prior to CVD, conductive Si wafer substrates were cleaned using acetone, isopropyl alcohol, H_2SO_4/H_2O_2 and rinsed in deionized water.

Substrates were then seeded with a nanodiamond dispersion (NanoAmando®B) in water (0.2 g L^{-1}) using a spin coater. At each B/C ratio two Si wafers were BDD coated, one was left "as-grown" and the second was CM polished. CM polishing was carried out using a Logitech Tribo polishing system in conjunction with a SUBA-X polishing pad and Logitech supplied Syton SF-1 alkaline colloidal silica polishing slurry containing 15-50 % SiO_2, 9.2 - 10.1 pH, 4-5 % ethylene glycol [28]. Samples were polished until the RMS roughness was reduced to < 2 nm. Samples grown with B/C ratios from 500 to 4000 ppm took 5 to 7 h, whereas the 8000 ppm sample took 2.5 h. An essential cleaning step followed CM polishing: BDD samples were dipped in HF (54 %) to remove any residual colloidal silica polishing slurry. Thus, in this study as-grown BDD electrodes and CM polished BDD electrodes after HF treatment are compared, representing the as-obtained surfaces.

2.2. Chemicals

Hexaammineruthenium(II) chloride, dopamine hydrochloride, ferrocene(I) methanol (FcMeOH), potassium hexachloroiridate(III) (all Sigma-Aldrich, Germany), potassium hexacyanoferrate(II) trihydrate, potassium hexacyanoferrate(III), potassium chloride, sodium dihydrogen phosphate dihydrate (all Lach-Ner, Neratovice, Czech Republic), and sodium hydroxide (Penta, Chrudim, Czech Republic) were of analytical grade and used without any further purification. Deionized water (Millipore Mili plus Q system, Billerica, USA) with resistivity of not less than 18.2 MΩ cm was used to prepare all aqueous solutions. 0.10 mol L^{-1} phosphate buffer of pH 7.4 was prepared by adjusting with 0.50 mol L^{-1} NaOH to desired pH value.

2.3. Characterisation techniques

Morphological characterization was investigated by AFM and SEM. AFM measurements were carried out at room temperature using a Bruker, Dimension Icon system in Peak Force Tapping mode with ScanAsyst Air tips (Bruker; k = 0.4 N m^{-1}; nominal tip radius 2 nm). Measured topographies have 512 x 512 points resolution. To obtain roughness data areas of 1 x 1 μm^2 and 5 x 5 μm^2 were analysed. SEM was carried out using a TESCAN FERA3 GM with Schottky field emission cathode. Several morphological examinations before and after polishing were performed at an acceleration voltage of 5 kV (secondary electron imaging), whereas microstructural crystallographic orientation mapping was performed at an acceleration voltage of 10 kV using an electron backscatter diffraction (EBSD) detector. Data was obtained using a EDAX DigiView V EBSD camera and EDAX APEX acquisition software, and subsequently processed with EDAX OIM Analysis 8 software containing a Neighbour Pattern Averaging & Reindexing (NPAR) tool.

Surface and bulk chemical analysis was carried out using Raman spectroscopy and XPS. Raman spectroscopy was carried out at room temperature using a Renishaw InVia Raman Microscope at

488 nm and with a laser power of 6 mW. For determination of boron concentration, [B] , the fitting tool at http://ofm.fzu.cz/raman-tool, which analyses characteristic Raman peaks at ca 1200 cm^{-1} and 1330 cm^{-1} attributed, respectively, to the Fano-shaped maximum of phonon density of states and zone-centre phonon line of heavily boron doped diamond, was used over the range of 1100 to 1500 cm^{-1}. Values for sp^3/sp^2 were obtained from fitting of Raman spectra, over the 1000-1700 cm^{-1} range, to obtain curve/peak integrated area values using Renishaw WiRe 3.2 software. Values were then used according to [33] to give a layer quality factor *fq* indicating sp^3/sp^2. XPS was carried out on a NanoESCA microscope (Omicron) using monochromatized Al Kα radiation (hν = 1486.7 eV). Peak deconvolution was made by KolXPD software with Voigt peaks on Shirley background. Overall instrumental resolution was 0.5 eV. XPS spectra of CM polished BDD were measured after HF treatment, while as-grown BDD measurements followed MW PECVD H plasma treatment to assure H-termination of the surface.

SECM measurements were carried out with a 920C system from CH Instruments (Austin/TX, USA). The instrument was positioned on a dampening plate in a custom-made Faraday cage. The laboratory-constructed electrochemical cell was made from polytetrafluoroethylene. A three-electrode setup was applied consisting of the SECM probe (as the working electrode), a Ag/AgCl/3 mol L^{-1} KCl reference electrode (CH Instruments, Austin/TX, USA), and a platinum wire as the counter electrode. Platinum disk electrodes with electrode diameters of 12.5 and 25 µm and an RG value (defined as the ratio of the total tip radius and the radius of the active microdisk electrode) of > 10 were used as SECM probes. BDD samples were mounted on the bottom of the electrochemical cell and the cell was levelled prior to imaging experiments. Measurements were conducted in 5 mL of a mediator solution (1.5 mmol L^{-1} of the respective mediator) with 1 mol L^{-1} KNO_3 as a supporting electrolyte. Solutions were not deaerated prior measurements. FcMeOH, ferrocyanide, ferricyanide, and hexaammineruthenium(III) were used as redox mediators. Probe approach curves (PACs) were measured at a fixed probe potential corresponding to the respective mediator: +0.3 V FcMeOH, +0.5 V for ferricyanide, +0.1 V for ferrocyanide, and −0.2 V for hexaammineruthenium(III). The maximum approach speed was 2.5 µm s^{-1} and quiet time was 15 s. Imaging experiments were conducted with the same fixed probe potentials, probe scan rate was 200 µm s^{-1}, and quiet time was 15 s. Areas covered in the images had a size of 500 x 500 $µm^2$ with a step size of 5 µm and were recorded in constant-height mode, corresponding to feedback currents of either 150 or 200 % relative to the steady-state current in the bulk solution. Determination of k^0_{app} values from SECM data was conducted according to the method reported by Wei *et al.* [34]. Several PACs per sample were conducted. Fitting of PACs with theoretical curves yields a k^0_{app} value per approached spot. The diffusion coefficient used for $[Ru(NH_3)_6]^{3+/2+}$ was 5.5×10^{-6} cm^2 s^{-1} [35]. PAC parameters were: probe potential -0.3 V, quiet time 15 s, maximum approach speed 0.5 µm s^{-1}.

For CV and SWV measurements a three-electrode setup was used consisting of an Ag/AgCl/3 mol L^{-1} KCl reference electrode and a platinum wire as an auxiliary electrode (both Elektrochemické detektory, Turnov, Czech Republic). The working electrode was constructed by Si wafers coated with the BDD layer placed in a Teflon electrode body with rubber sealing. The exposed geometrical area of the electrode was 2.01 mm^2.

CV measurements were performed using an Eco-Tribo polarograph with PolarPro 5.1 software (Eco-Trend Plus, Czech Republic). SWV experiments were carried out using a Palm-Sens potentiostat with PSTrace 5.8 software (PalmSens BV, Houten, The Netherlands) using optimized parameters (amplitude A, frequency f, potential step ΔE_s) for (i) as-grown BDD_{500}: A = 60 mV, f = 20 Hz, ΔE_s = 8 mV, (ii) as-grown BDD_{4000}: A = 50 mV, f = 10 Hz, ΔE_s = 4 mV, (iii) CM polished BDD_{500}: A = 120 mV, f = 10 Hz, ΔE_s = 8 mV, and (iv) CM polished BDD_{4000}: A = 220 mV, f = 20 Hz, ΔE_s = 3 mV. EIS measurements were carried out using Autolab PGSTAT101 potentiostat with Nova 2.1 software (Metrohm Autolab B.V., Utrecht, The Netherlands). Impedance spectra were recorded in 1 mol L^{-1} KCl at a potential 0 V, amplitude 10 mV and within the frequency range from 100 kHz to 0.1 Hz. Data were fitted by the equivalent circuit (depicted in Fig. S10a) containing constant phase element (CPE) and the parameters N and Y_0 were evaluated. To normalize the Y^0 values the real surface areas A_{real} calculated from AFM measurement were used. EIS data in 1 mol L^{-1} KCl in the presence of 1 mmol L^{-1} $[Fe(CN)_6]^{3-/4-}$ were measured at the potential E = +0.25 V and were evaluated using the equivalent circuit depicted in Fig. S11a). Obtained CPE values only in 1 mol L^{-1} KCl worked as the reference values during the fitting in the presence of the 1mmol L^{-1} $[Fe(CN)_6]^{3-/4-}$ redox system.

Concentration dependencies for dopamine were constructed from the average of five replicate measurements for each concentration on each BDD electrode.

The apparent heterogenous electron transfer rate constant k^0_{app} was calculated by the Nicholson method [36], based on the difference in potential of the anodic and cathodic peaks ΔE_p of redox species according to Equation (1),

$$k^0_{app} = \psi\left[\frac{\pi D_0 n F v}{RT}\right]^{1/2} \quad (1)$$

where ψ is a dimensionless parameter obtained from the logarithmic dependence of ψ on ΔE_p evaluated from CVs [36], D_0 is the diffusion coefficient, n is the number of electrons, F is the Faraday constant (C mol^{-1}), υ the scan rate (V s^{-1}), R is the gas constant (J K^{-1} mol^{-1}), T is the temperature (K), and the value of π is 3.14. Further, k^0_{app} values were calculated from Tafel plots using Equation (2),

$$i^0 = nFA_{real}k^0_{app}c \quad (2)$$

where i^0 is the exchange current obtained from Tafel plots (A), n is number of electrons, F is Faraday constant (C mol^{-1}), A_{real} is the real exposed BDD area (cm^2), k^0_{app} is kinetic constant (cm s^{-1}), c is concentration (mol cm^{-3}).

The following diffusion coefficients were used for particular redox markers: 7.6×10^{-6} cm^2 s^{-1} for $[Fe(CN)_6]^{3-/4-}$ [37], 5.5×10^{-6} cm^2 s^{-1} for $[Ru(NH_3)_6]^{3+/2+}$ [35] and 8.3×10^{-6} cm^2 s^{-1} for $[IrCl_6]^{2-/3-}$[38]. Limits of detection (*LOD*) for SWV determination of dopamine were calculated as threefold of the standard deviation *s* of the peak currents (n = 7) of the lowest measurable concentration divided by the slope of corresponding concentration dependence.

3. Results and Discussion

3.1. Nano-structural characterisation of BDD electrodes

AFM and SEM were used to obtain the micrographs of each as-grown and CM polished BDD electrode. Fig. 1 displays micrographs for BDD_{500}, BDD_{1000}, BDD_{2000}, BDD_{4000} and BDD_{8000} electrodes. The images for as-grown electrodes typically show a well-defined crystalline structure with well-defined facets up to a B/C ratio of 4000 ppm. At 8000 ppm the crystalline quality and grain size is diminished with a high grain boundary content. It is a well-known phenomenon that the grain size decreases as the boron concentration is increased beyond saturation [39]. This figure clearly highlights the change in morphology following CM polishing of the BDD layers. After the polishing the layer exhibits not only a smooth surface, but also a well-defined grain boundary content. SEM micrographs clearly show that following CM polishing, BDD grains contain numerous growth twins. Cross-sectional SEM images (see Fig. S1) show that only the minimum of material was removed during the CM polishing step. AFM RMS roughness measurements confirm that the roughness following CM polishing is dramatically reduced, see Tab. 1. In all cases, except one, the roughness is at or below 2 nm. The RMS roughness value for BDD_{1000} is affected by holes in the layer, leading to an increase in measured roughness. These holes are most likely related to remnants of the original surface roughness. When investigated over a smaller area (1 µm × 1 µm) the RMS roughness for BDD_{1000} was found to be also < 2 nm. The reduced RMS roughness of the as-grown BDD_{8000} sample was reflected by the reduced CM polishing time, *i.e.*, less material was needed to be removed to reduce the RMS roughness to < 2 nm.

Tab. 1. RMS roughness and real surface area vales from AFM (5 µm × 5 µm) measurements of as-grown (AG) and CM polished (CMP) BDD electrodes.

Sample	AFM – RMS roughness (nm)		Surface area difference (%)		A_{real} (cm^2)	
	AG	CMP	AG	CMP	AG	CMP
BDD_{500}	25	1.3	17.1	0.0291	0.0235	0.0201
BDD_{1000}	32	6.2	19.2	1.18	0.0240	0.0203
BDD_{2000}	32	1.5	18.1	0.0507	0.0237	0.0201
BDD_{4000}	54	2.2	37.7	0.199	0.0277	0.0201
BDD_{8000}	15	0.6	17.5	0.0561	0.0236	0.0201

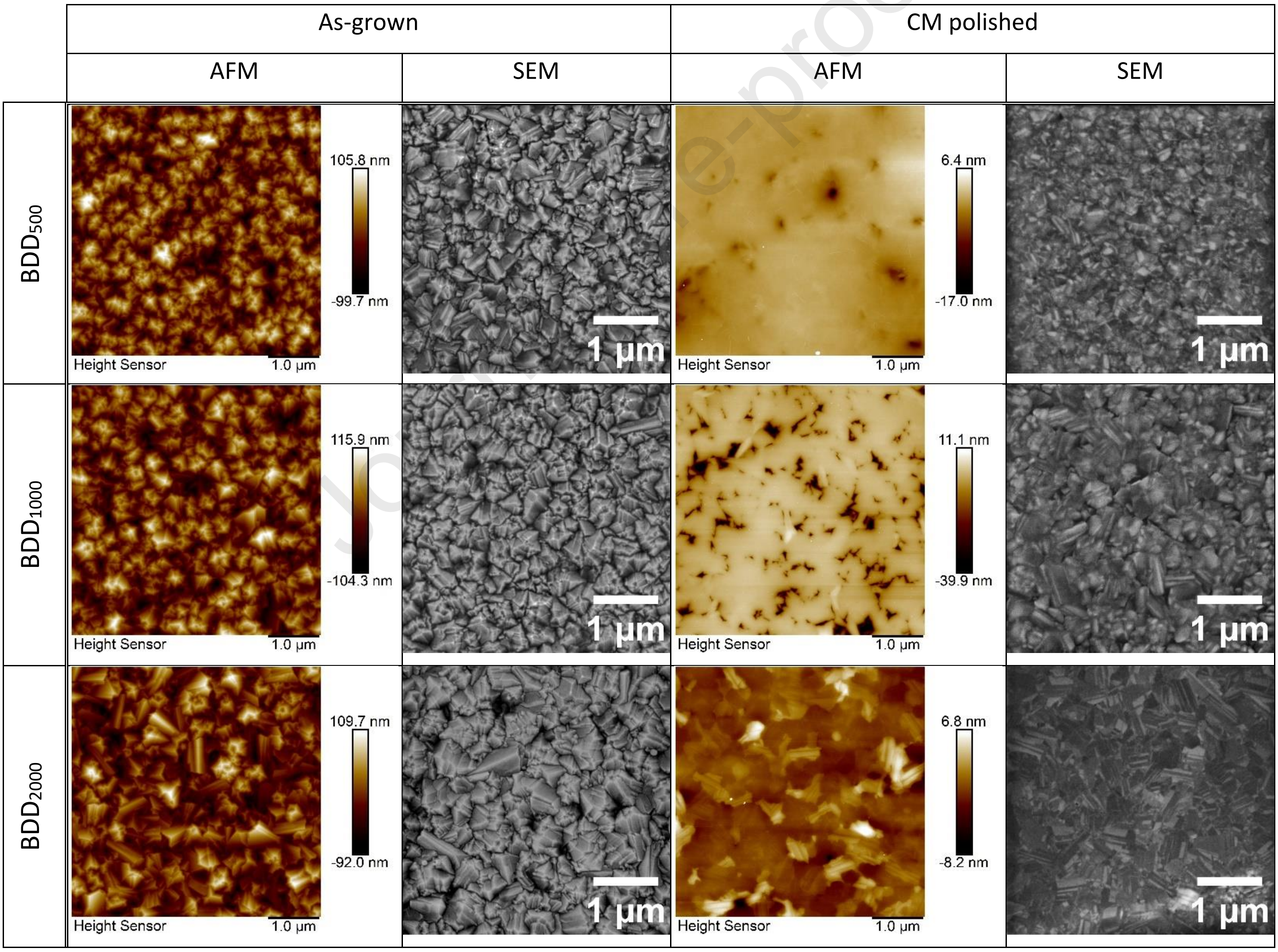

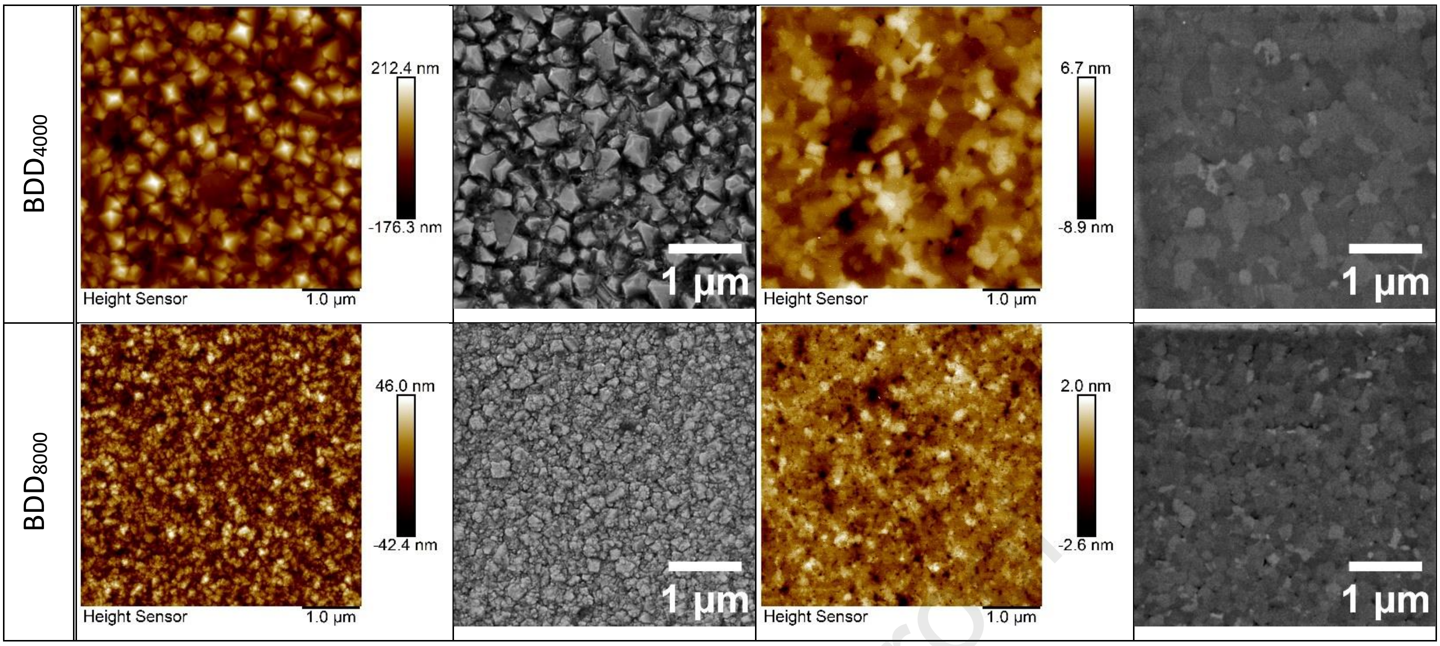

Fig. 1. AFM and SEM micrographs of as-grown and CM polished BDD_{500}, BDD_{1000}, BDD_{2000}, BDD_{4000} and BDD_{8000} electrodes.

Orientation mapping using EBSD was carried out on the CM polished BDD_{2000} sample. The high-quality CM polishing and signal collection conditions enabled the acquisition of Kikuchi patterns on ultra-thin BDD layers, we believe, for the first reported time, however their acquisition remains complicated on diamond samples. Therefore, the conventional approach for this method was modified for such material. An example of a Kikuchi pattern can be seen in Fig. 2a) and an orientation map of the surface in Fig. 2b). After data processing using available tools (NPAR, pattern contrast improvement and indexation filtering) there is a visible equiaxed microstructure with a Gaussian grain size distribution, Fig. 2c). The grain size was measured to be 0.3 ± 0.1 µm. Grain orientations are not distributed randomly, but instead a strong texture is present with the strongest component having {011} along with a contribution from {111}, Fig. 2d).

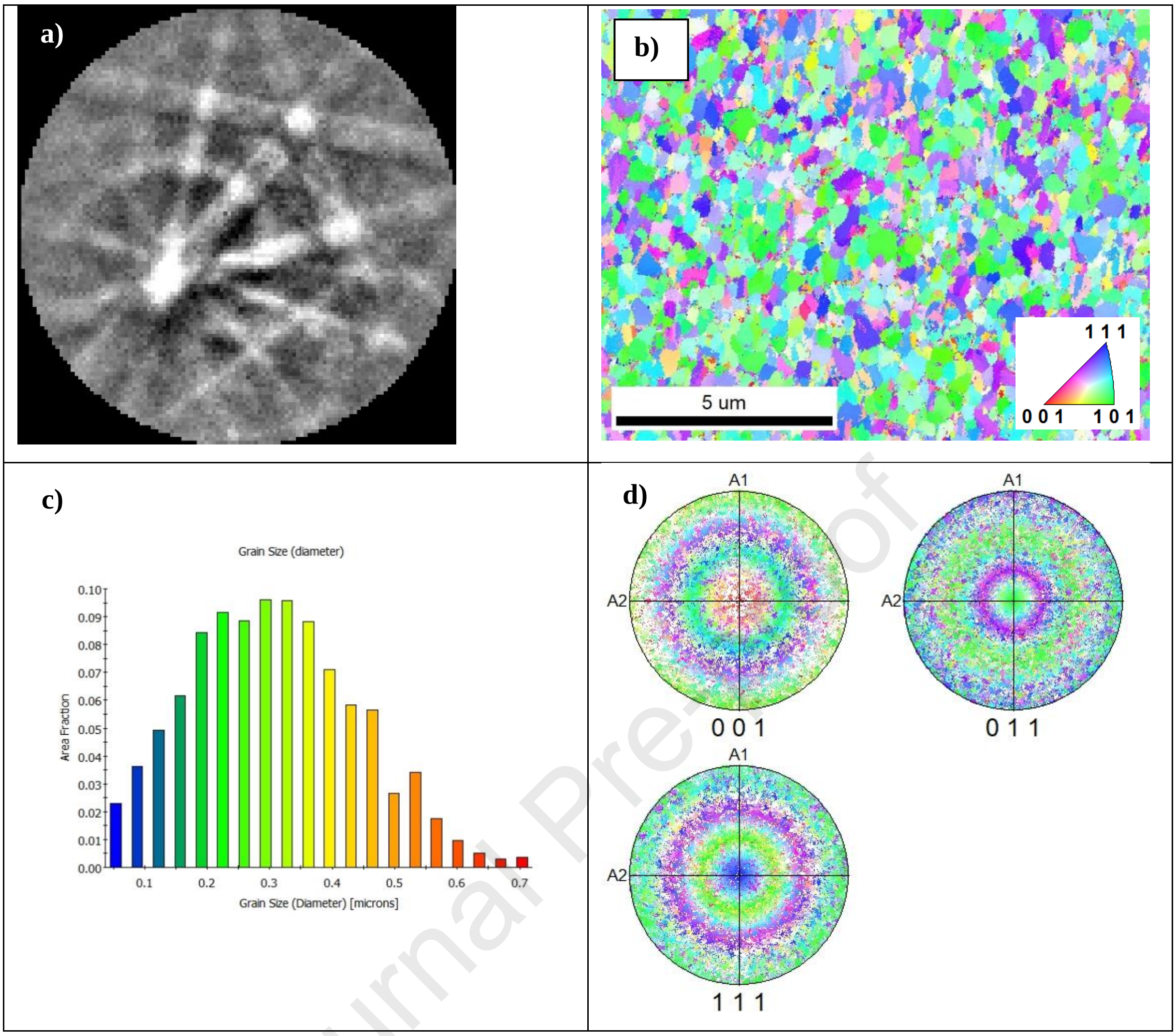

Fig. 2. Orientation Image Maps of CM polished BDD_{2000} electrode: a) example of obtained Kikuchi pattern; b) grain orientation map; c) grain size distribution histogram; d) pole figures for {001}, {011} and {111} planes.

3.2. Spectral characterisation of BDD electrodes

Raman spectroscopy is a useful tool for estimating the composition of BDD layers. It is capable of evaluating the boron doping level, which is incorporated in the layers, as well as the presence of non-diamond carbon. Fig. S2 shows typical Raman spectrum for low to high boron containing electrodes with boron related bands at *ca* 480 cm^{-1} and 1200 cm^{-1}, and a red shifted (from *ca* 1330 cm^{-1} down to *ca* 1282 cm^{-1}) Fano shaped diamond Raman line. The contribution from non-diamond phase bands at 1520 cm^{-1} can be seen to be rather constant with B/C ratios up to 2000 ppm, at 4000 and 8000 ppm this contribution increases. In addition, peaks related to the Si substrate are visible at 520 cm^{-1} and 950 cm^{-1}. The diamond red shift is increasing with higher boron doping levels and is associated with phonon confinement effect caused by the high concentration of boron defects and negative asymmetric coefficient with the Fano effect. The determined [B] concentration was established to be from 0.58×10^{21} cm^{-3} for BDD_{500} electrodes up to 4.4×10^{21} cm^{-3} for BDD_{8000} electrodes [40,41], for exact values of as-grown and CM polished BDD see Tab. S1. All values are above the theoretical threshold of [B] ≈ 2×10^{20} cm^{-3} for metallic-like conductivity [11]. After CM polishing the Raman spectra remained the same without any significant change (see Fig. S2).

XPS was carried out on all as-grown and CM polished BDD electrodes, obtained O 1s, C 1s and B 1s spectra are depicted in Fig. 3. They show the elementary content to be 98.9 - 95.7 %, 0.23 – 4.79 % and 0.7 - 1.9 %, respectively in as-grown samples. After CM polishing, a rise in oxygen content, 4.4 – 6.3 %, is observed, as summarized in Tab. 2. This can be expected following the strong oxidizing hydrofluoric acid cleaning step, applied to remove any residual silica slurry used for CM polishing, and may also support the proposed mechanism of polishing in [28], which suggests that due to wet oxidation of the surface during CM polishing, the amount of carbonyl and hydroxyl groups increases on the surface. In the samples with the highest B doping, the content of B rose by 0.3 – 1 % of the total. Figs. S3a-c) show, as an example, detailed fitting of O 1s, C 1s and B 1s spectra for the BDD_{2000} electrodes as-grown and after CM polishing. Fitting of the O 1s spectra for both electrodes provide two components. Peak I. can be assigned to C-O and the peak II. is likely related to COOH functional groups [42]. C 1s spectra show several peaks. Peak I. corresponds probably to B_4C or B_3C. Peaks II. and III. are difficult to separate especially on CM polished electrodes, but these peaks can be attributed to sp^2 or sp^3 carbon C-C bonds and peak IV. to sp^3 C-H bonds [43]. Peak V. correlates with C-O. The final visible peak VI. occurring only on CM polished electrodes is related to COOH functional groups [12,44,45]. Following CM polishing C 1s spectra shows an overall increase in sp^2/sp^3 carbon content. This may be caused by introduction of C=O functional groups on the surface layer. B 1s spectra shows three peaks where peak I. may correspond to boron clusters, and peaks II. and III. correlate with B-C and B-H bonds respectively. The increase in [B] content of the highest doped electrodes after CM polishing could contribute to the explanation of the improved electrochemical performance and overall conductivity, as demonstrated below. An explanation for this could be a "shut-down" effect, where diamond deposition continues during the switch off procedure following CVD, *i.e.*, reduction in microwave power and gas flows, leading to a surface with lower [B], which after CM polishing reverts to the bulk [B] content. Overall, it can be said that CM polished electrodes have a higher surface quality (lower inelastic background in spectra and higher and narrower peaks comparing to the as-grown electrode) in comparison to the as-grown electrodes.

The evaluation of data obtained from Raman and XPS measurements enables further estimation of [B] values and a rough evaluation of sp^2 carbon content. The values obtained using both methods are listed in Tab. S1. [B] bulk (Raman) and surface (XPS) values match quite well, with the same trend, *i.e.*, [B] increases with B/C as obvious from Fig. S4a). Bulk [B] values are consistent for as-grown and CM polished electrodes. The same can be said for surface [B] values at low B/C, whereas at higher B/C (4000 and 8000 ppm) there is a clear increase in [B] following CM polishing, due to the mentioned "shut-down" effect.

The qualitative value of bulk sp^3/sp^2 from Raman is indicated by layer quality factor *fq.* The contribution from non-diamond carbon at 1520 cm^{-1} can be seen to be rather constant in as-grown and CM polished electrodes with B/C ratios up to 2000 ppm ($fq \geq 96$), at 4000 and 8000 ppm this contribution increases ($fq \leq 93$) as seen in Fig. S4b). For XPS, to give a qualitative value for surface sp^3/sp^2 fitting was attempted on the C 1s spectrum. However, fitted peaks, II. (sp^2) + III. & IV. (sp^3), are not fully resolved leading to highly speculative values, from which no clear trend appears, see Fig. S4b). If peak I. at ~ 283 eV, is assumed to be sp^2 related, as in [46] or at least partly related, then a trend can be found, *i.e.*, that sp^2 content increases with B/C, see Fig. S4c) This agrees with Raman data, *i.e.*, decrease in sp^3/sp^2 with increasing B/C, and SEM observations, *i.e.*, reduction in grain size and hence larger grain boundary content, especially when B/C = 8000 ppm. However, as further discussed in the Section 3.4, no sp^2 related features are visible from an electrochemical point of view, therefore it is not clear how relevant or reliable these findings are.

Tab. 2. Values for C, B and O as measured by XPS of as-grown (AG) and CM polished (CMP) BDD electrodes.

Sample	C (%)		B-C contribution to C (%)		B (%)		O 1s (%)	
	AG	CMP	AG	CMP	AG	CMP	AG	CMP
BDD_{500}	97.9	95.4	0.23	0.22	0.25	0.19	1.9	4.4
BDD_{1000}	98.9	94.4	0.56	0.55	0.41	0.33	0.7	5.3
BDD_{2000}	97.7	93.7	1.14	1.01	0.67	0.66	1.6	5.7
BDD_{4000}	96.3	91.8	3.57	4.14	2.41	2.68	1.3	5.6
BDD_{8000}	95.7	90.0	4.79	5.25	2.71	3.69	1.6	6.3

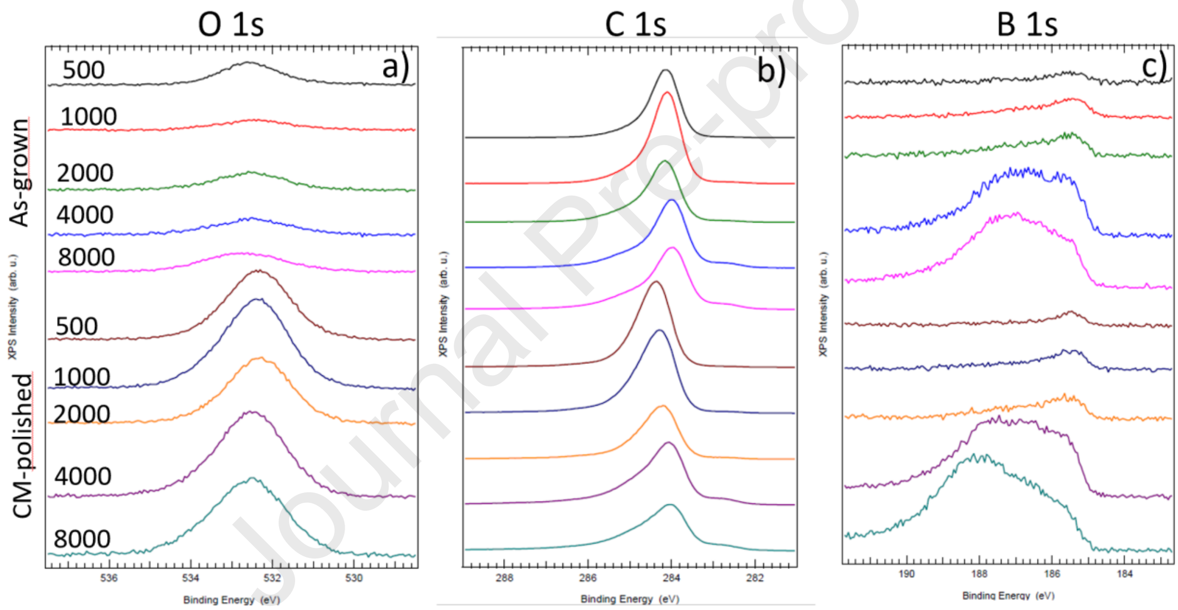

Fig. 3. a) O 1s, b) C 1s and c) B 1s XPS spectra of all investigated electrodes, in the order from top to bottom: As grown $BDD_{500\ to\ 8000}$ and CM polished $BDD_{500\ to\ 8000}$

3.3. Scanning electrochemical microscopy

Feedback mode in SECM was utilised to investigate the electrochemical surface activity of BDD electrodes on the microscale. These measurements were performed in 1 mol L^{-1} KNO_3 at substrate potentials where surface interaction of the NO_3^- ions with C-H on the surface [47] of BDD presumably do not influence the electrochemical activity. The topographical influence on the SECM signal could be ruled out, as AFM measurements confirmed that the surface roughness were on the nm scale. Therefore, SECM measurements were performed in constant-height mode. At first, four commonly used redox mediators were evaluated for their suitability. Fig. S5 shows SECM images of the same area on the as-grown BDD_{4000} sample recorded in different mediator solutions. By using outer-sphere redox mediators (FcMeOH and hexaammineruthenium(III)), surface details could be resolved well, while use of inner-sphere redox mediators (ferri- and ferrocyanide) resulted in rather poor image quality. The same experiments were also conducted on the CM polished BDD_{4000} electrode, here the image quality recorded with the outer-sphere mediators was comparable to the ones with the inner-sphere mediators. Further comparison of the two sets of BDD electrodes was carried out with FcMeOH, since it resulted in the overall highest image quality. In Fig. 4, typical PACs toward the as-grown BDD_{8000} electrode and a SECM image are shown. During the approach toward the surface, positive as well as mixed feedback was observed. The red PAC in Fig.4 a) shows a PAC with positive feedback, typical for a conductive surface. In contrast, the blue PAC indicates an initial slight increase in the current when approaching the sample surface followed by a sharp current decrease near the BDD surface, resulting in negative feedback, typical for an insulating surface. This behaviour was found solely on as-grown electrodes and not on CM polished electrodes. In Fig. 4 b) the corresponding destinations of the PACs are highlighted in red and blue.

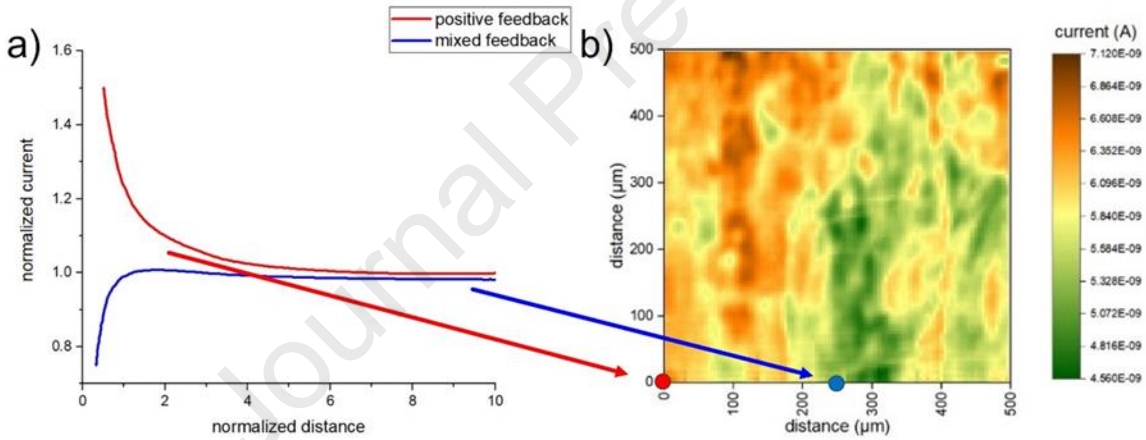

Fig. 4. **a)** PACs toward the surface of the as-grown BDD_{8000} electrode. Positive (red line) as well as mixed feedback (blue line) was observed during the approach. **b)** SECM image of the as-grown BDD8000 electrode with the corresponding positions for the PACs in **a)**. Measurements were conducted in 1.5 mmol L^{-1} FcMeOH in 1 mol L^{-1} KNO_3, electrode diameter = 25 µm. Probe potential +0.3 V, quiet time was 15 s. Feedback current of 150% relative to the current in the bulk solution. Arrows and points in red and blue indicate the approach positions corresponding to the feedback behaviour shown in 4 a).

In Fig. 5, SECM images of the surface of as-grown and CM polished BDD_{500}, BDD_{2000}, and BDD_{8000} electrodes are shown in uniform normalized current scale. The surface activity of as-grown BDD was shown to be heterogeneously distributed, exhibiting spots of high electrochemical activity, mixed with spots of insulating properties. As expected, with increasing boron doping, the number of conductive spots increased. CM polishing was found to lead to a much more uniform distribution of surface activity, especially at high boron doping. It is known that boron atoms are uniformly distributed in depth of BDD layers regardless of boron concentration, as confirmed by secondary ion mass spectrometry and elastic recoil detection [43–45]. The exposure of uniformly distributed bulk boron atoms on the surface of CM polished electrodes is thus reflected in uniformity of their conductivity. However, still the CM polished samples were shown to have some variation in this electrochemical activity as is obvious from Fig. S6, which shows SECM images with a narrower current scale.

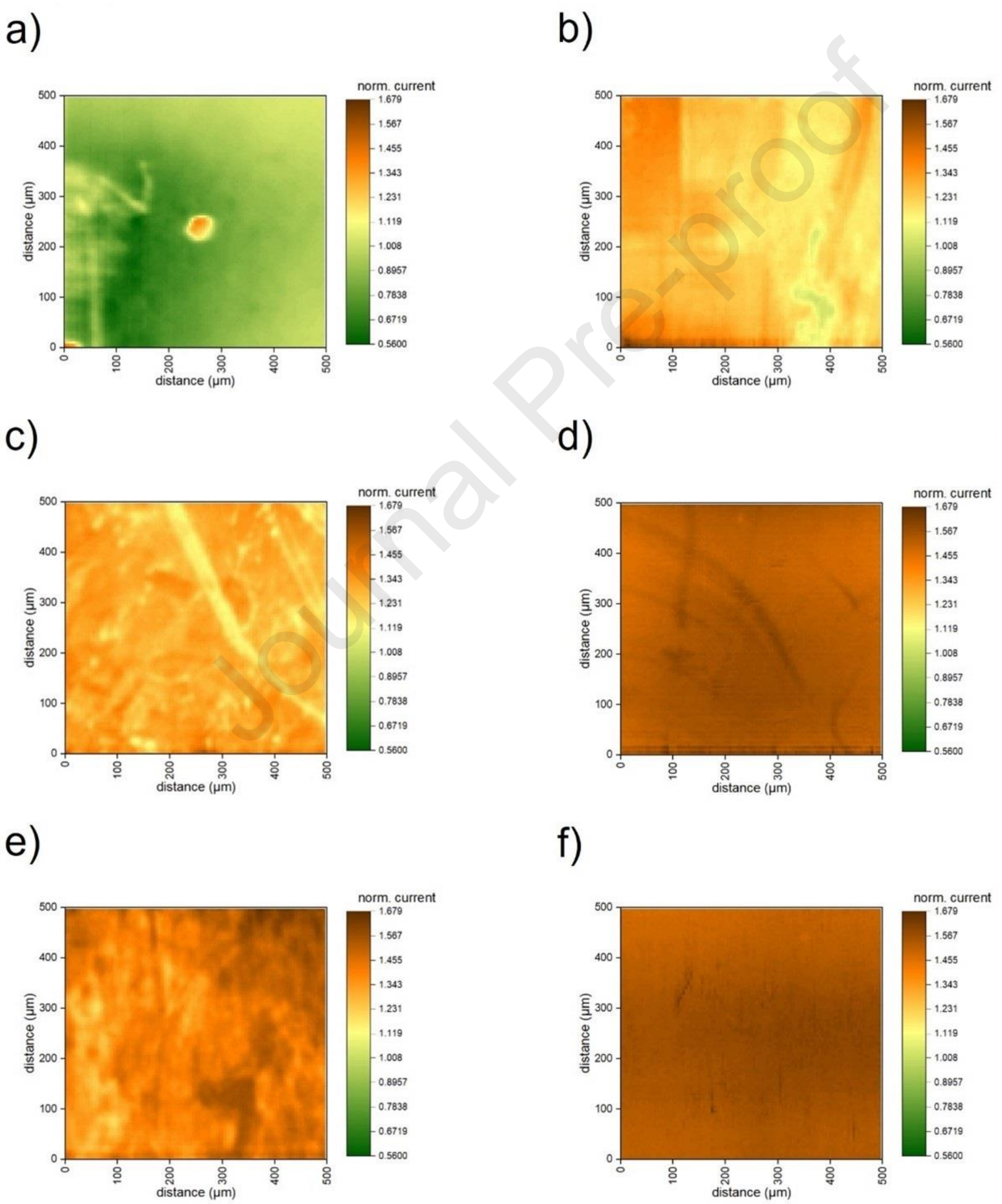

Fig. 5. SECM images of as-grown and CM polished BDD electrodes: a) as-grown BDD_{500}, b) CM polished BDD_{500}, c) as-grown BDD_{2000}, d) CM polished BDD_{2000}, e) as-grown BDD_{8000}, f) CM polished

BDD_{8000}. Measurements were conducted in a 1.5 mmol L^{-1} FcMeOH in 1 mol L^{-1} KNO_3, electrode diameter = 25 µm. Probe potential +0.3 V, quiet time was 15 s. Imaging was done at a constant height corresponding to a feedback current of 150% relative to the current in the bulk solution. Current scale was normalized to the bulk current signal.

The range of k^0_{app} values further characterizing electrochemical surface activity was calculated from seven individual PACs towards different positions on the BDD_{4000} electrodes. For as-grown BDD, k^0_{app} values ranging from 0.113 up to 0.313 cm s^{-1} were calculated, while for CM polished BDD_{4000} electrode the values yielded a range from 0.280 to 0.382 cm s^{-1}. Overall, the CM polished sample seems to have a higher electrochemical activity, as well as a more homogeneous distribution shown by a narrower range of k^0_{app} values. Homogeneity is also expressed by the lower variance of k^0_{app} values for CM polished in comparison with as-grown BDD.

3.4. Electrochemical characterization of BDD electrodes

Electrochemical characterization of as-grown BDD and CM polished BDD electrodes (BDD_{500} – BDD_{8000}) was performed to evaluate the effect of surface smoothing on HET kinetics and capacitance obtained from EIS measurements. CV measurements in 1 mol L^{-1} KCl in the presence of outer- ($[IrCl_6]^{2-/3-}$ and $[Ru(NH_3)_6]^{3+/2+}$) and inner-sphere ($[Fe(CN)_6]^{3-/4-}$, dopamine/dopamine-*o*-quinone) redox markers were performed for this purpose. The surface of the electrodes was kept in the as-grown and as-polished states (after HF treatment to remove residual silica used for CM polishing) by avoiding potentials leading to water electrolysis and thus surface oxidation/reduction. Re-hydrogenation of the CM polished surface was not attempted, as the stability of H-termination obtained using cathodic polarization or H-plasma treatment and their effectiveness for CM polished BDD has not been studied yet and thus is questionable especially in long-term studies, therefore here we focus on the as-obtained surfaces.

The reversibility of the redox reactions for inner/outer-sphere redox probes was examined based on the values of peak potentials difference of anodic and cathodic peak (ΔE_p) and I_{pA}/I_{pC} ratio of peak currents of anodic/cathodic signal. ΔE_p values are summarized in Tab. 3, I_{pA}/I_{pC} values are listed only for dopamine/dopamine-*o*-quinone (see Tab. 4) because for other markers they were close to 1.0. Further, values of apparent heterogeneous electron transfer rate constant k^0_{app} calculated by the Nicholson method from ΔE_p values [36] for all tested inorganic redox markers were estimated and are reported in Tab. 3.

Fig. 6 represents an example of CV measurements of outer-sphere ($[Ru(NH_3)_6]^{3+/2+}$) and inner-sphere ($[Fe(CN)_6]^{3-/4-}$) probe in 1 mol L^{-1} KCl on all as-grown and CM polished BDD electrodes at a scan rate of 0.1 V s^{-1}. For outer-sphere redox markers reversible or nearly reversible behaviour was observed on all electrodes independent of boron doping level and surface morphology, characterized by ΔE_p values ranging from 60 mV to 71 mV for $[Ru(NH_3)_6]^{3+/2+}$ (CVs in Fig. 6 a), b)) and from 55 mV to 66 mV for $[IrCl_6]^{2-/3-}$. For both markers, CM polishing led to unification of ΔE_p values (difference in ΔE_p only 5 mV among the individual electrodes differing in boron doping level). k^0_{app} values reflect the minimal differences in ΔE_p and lay within one order of magnitude from 0.201 cm s^{-1} to 0.019 cm s^{-1} for both as-grown and CM polished BDD electrodes.

Obviously, the HET kinetics for outer-sphere redox markers on as-grown and CM polished surface is neither influenced by boron doping level nor on surface morphology and is determined by the electron transfer from the solution species to electrode. This transfer is not hindered by the chemical species terminating the BDD surface, *i.e.*, a slightly higher content of oxygenous groups as shown by XPS measurements. Similar insensitivity was reported in our previous study on as-grown surfaces for BDD layers differing in boron content [48] or deposited in various MW PECVD systems [49]. This confirms sufficient conductivity even for lower doped BDD electrodes thanks to the dominant H-terminated surface and relative low oxygen content, slightly increased after CM polishing. Increased ΔE_p values differing from 59 mV for $[Ru(NH_3)_6]^{3+/2+}$ redox probe were reported for O-terminated surfaces and low boron content in BDD layers deaccelerating HET kinetics [14,16]. Values lower than 59 mV were attributed to increased sp^2 carbon content with attached oxygen functionalities bearing partially negative charge thus supporting adsorption of the positively charged $[Ru(NH_3)_6]^{3+/2+}$ redox marker recognized in porous BDD layers [44] or the effect of thin layer diffusion know from other carbon porous materials [50–52].

However, the changes in HET kinetics due to CM polishing procedure are clearly visible using surface-sensitive inner-sphere redox marker $[Fe(CN)_6]^{3-/4-}$. While ΔE_p values for as-grown BDD electrodes range from 429 mV to 228 mV, CM polished BDD electrodes display substantially lower values ranging from 100 mV to 75 mV (CVs in Fig. 6 c), d)) and characteristics in Tab. 3. Fig. S7b) represent the expected decline in ΔE_p values with increasing [B] estimated from Raman. In general, ΔE_p values for $[Fe(CN)_6]^{3-/4-}$ on BDD electrodes increase with increasing oxygen content (due to interaction of the redox marker with π electrons present in oxygenous groups [53]) and decreasing boron content [11,12,48,54]. For the as-grown BDD electrodes, higher values of ΔE_p for $[Fe(CN)_6]^{3-/4-}$ on the lower doped layers indicate a limited number of charge carriers, *i.e.*, boron-rich sites eventually blocked by the presence of oxygenous groups. Clearly CM polishing leads to dramatic acceleration of HET kinetics, which is more pronounced for low doped BDD electrodes. This might be due to the uniform distribution of boron atoms recognized by uniform electrochemical activity in SECM for BDD_{500} – BDD_{2000} electrodes together with a relative increase in boron concentration on the surface after CM polishing for BDD_{4000} and BDD_{8000}, as seen in XPS measurements. The increase in HET kinetics is characterized by k^0_{app} values from 0.005 cm^2 s^{-1} (500 ppm) to 0.019 cm^2 s^{-1} (8000 ppm) on CM polished surfaces. k^0_{app} values for $[Fe(CN)_6]^{3-/4-}$ were further evaluated from Tafel plots (depicted in Fig. S8, k^0_{app} values listed in Tab. 3) for all as-grown and CM polished BDD electrodes. All evaluated kinetic and thermodynamic parameters are listed in Tab. S2. E^0 values are ~ +0.273 V for all studied BDD films. Tafel slopes varied around 118 mV per decade for as-grown BDD films, which correlates with a 1e^- process. For CM polished BDD electrodes they range from 105 – 152 mV per decade. This can be explained by accelerated HET kinetics on the CM polished BDD electrodes in comparison with as-grown ones and therefore complicated and inaccurate evaluation of Tafel slopes. The values of transfer coefficient α and β are around 0.5 which indicates the symmetry of kinetics of the oxidation/reduction reaction. Evaluation of Tafel slopes enables calculation of k^0_{app} values for all as-grown BDD electrodes even for those with lower boron doping levels (500, 1000 and 2000 ppm), not assessed by Nicholson method. For as-grown BDD films, k^0_{app} values vary from 0.00044 to 0.00163 cm s^{-1} for BDD_{500} to BDD_{8000}, *i.e.,* roughly increase with increasing boron doping level and are comparable with the values of k^0_{app} calculated by the Nicholson method for BDD_{4000} and BDD_{8000}. The values calculated for CM polished electrodes are in general higher, about 0.006 cm s^{-1} for BDD_{500} and BDD_{1000}, *i.e.,* comparable with values calculated by Nicholson method. For CM polished electrodes with higher doping level, they increase to 0.0075 cm s^{-1} documenting faster HET kinetics, however these values are lower than that estimated by Nicholson, which can be caused by complicated Tafel slope evaluation as mentioned above. The last method used for calculation of k^0_{app} is based on evaluation of PAC curves obtained from SECM measurements. When we compare k^0_{app} values obtained from SECM using $[Ru(NH_3)_6]^{3+/2+}$ as redox probe (see Section 3.3) with k^0_{app} values obtained from CV measurements for BDD_{4000} electrodes using outer and inner sphere probes the same trend can be seen, *i.e.* higher k^0_{app} values on CM polished in comparison with as-grown BDD surfaces. The absolute k^0_{app} values evaluated from SECM also show a lower variance for CM polished BDD electrodes confirming lower heterogeneity in electrochemical activity of the surface.

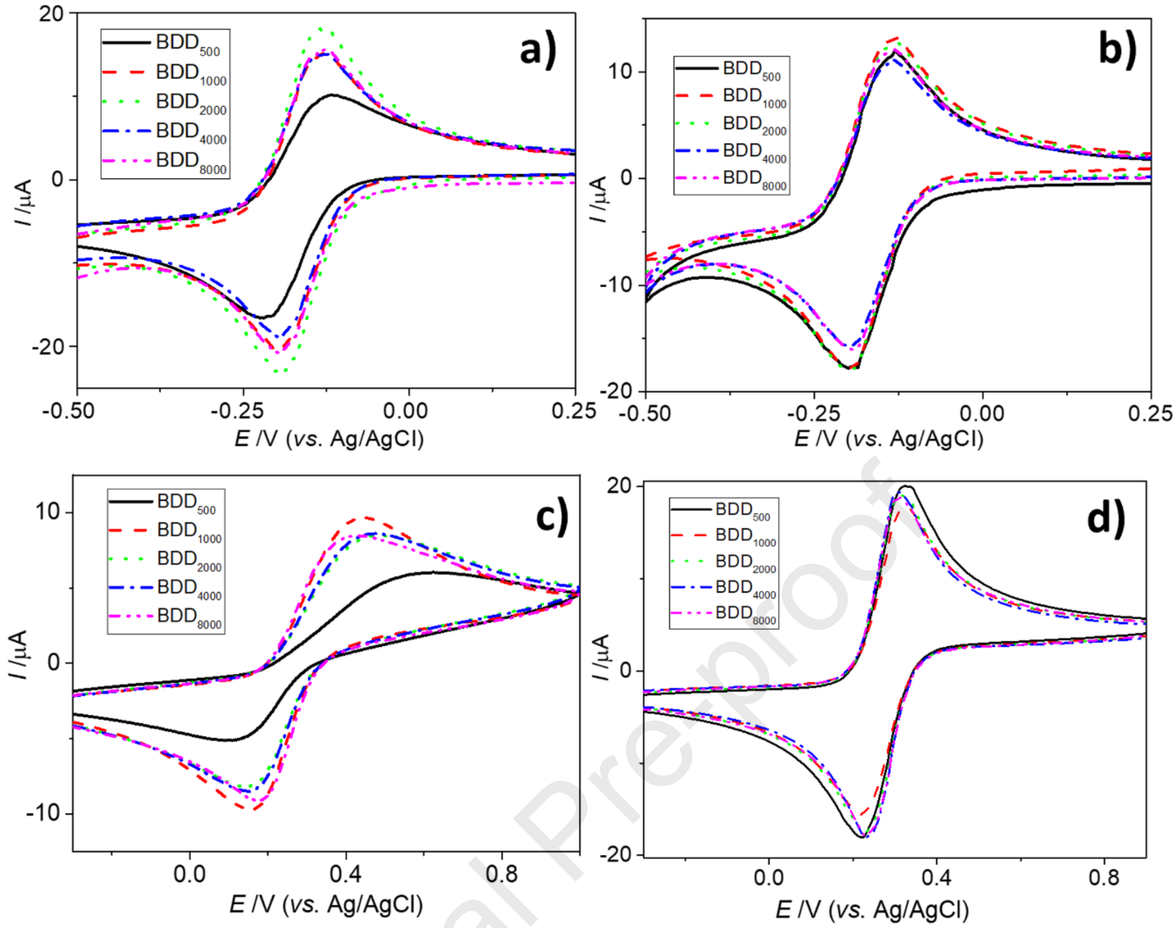

Fig. 6. Cyclic voltammograms of **a)** 1 mmol L^{-1} $[Ru(NH_3)_6]^{3+/2+}$ and **c)** 1 mmol L^{-1} $[Fe(CN)_6]^{3-/4-}$ on as-grown BDD electrodes, and **b)** 1 mmol L^{-1} $[Ru(NH_3)_6]^{3+/2+}$, **d)** 1 mmol L^{-1} $[Fe(CN)_6]^{3-/4-}$ on CM polished BDD electrodes. Supporting electrolyte 1 mol L^{-1} KCl, scan rate 0.1 V s^{-1}.

Tab. 3 Calculated ΔE_p and k^0_{app} values for inorganic redox markers, Y^0 and N values of CPE estimated by EIS in 1 mol L^{-1} KCl at 0 V and R_{ct} estimated by EIS in 1 mmol L^{-1} $[Fe(CN)_6]^{3-/4-}$ at +0.25 V on as-grown (AG) and CM polished (CMP) BDD_{500} – BDD_{8000} electrodes.

	Cyclic voltammetry						Electrochemical impedance spectroscopy					
Marker	$[Ir(Cl_6)]^{2-/3-}$		$[Ru(NH_3)_6]^{3+/2+}$		$[Fe(CN)_6]^{3-/4-}$		1 mol L^{-1} KCl				1mmol L^{-1} $[Fe(CN)_6]^{3-/4-}$	
	AG	CMP	AG	CMP	AG	CMP	AG		CMP		AG	CMP
Sample	ΔE_p (mV)						[b]Y^0	N	[b]Y^0	N	R_{ct} (kΩ)	R_{ct} (kΩ)
BDD_{500}	66	55	71	65	429	100	4.50	0.977	12.0	0.973	278	3.17
BDD_{1000}	57	55	63	60	270	100	5.01	0.955	27.1	0.894	52.7	2.7
BDD_{2000}	60	60	63	60	297	85	8.05	0.937	17.1	0.963	38.7	1.56
BDD_{4000}	63	60	63	60	225	75	14.7	0.936	37.2	0.923	14.7	0.579
BDD_{8000}	66	55	69	60	228	75	13.2	0.907	40.8	0.923	14.9	0.45
k^0_{app} (cm s^{-1})			Nicholson method				Tafel plots for		$[Fe(CN)_6]^{3-/4-}$			
BDD_{500}	0.040	0.201	0.019	0.041	[a]–	0.005	0.00046		0.00634			
BDD_{1000}	0.201	0.201	0.057	0.164	[a]–	0.005	0.00137		0.00534			
BDD_{2000}	0.201	0.201	0.057	0.164	[a]–	0.010	0.00107		0.00679			
BDD_{4000}	0.071	0.201	0.057	0.164	0.001	0.019	0.00098		0.00710			
BDD_{8000}	0.040	0.201	0.022	0.164	0.001	0.019	0.00163		0.00728			

[a] For ΔE_p values above 212 mV the dimensionless parameter ψ isn't defined thus k^0_{app} couldn't be calculated.

[b] The units of Y^0 values are μMho $s^{-1}cm^{-2}$

The impedance of the CPE is provided by: $Z_Q = \frac{1}{Y_O(j\omega)^n}$

Both methods for evaluation of HET kinetics witness its acceleration for surface sensitive $[Fe(CN)_6]^{3-/4}$ due to CM polishing. Clearly, the slight increase in oxygenous groups on CM polished electrodes is not the main factor influencing HET kinetics. The same is valid for the content of non-diamond phase, as shown in Fig. S7a) depicting the dependence of ΔE_p values for redox markers on sp^3/sp^2 evaluated from Raman measurements. Only minor differences in ΔE_p values can be recognized for outer sphere markers and $[Fe(CN)_6]^{3-/4-}$. Clearly CM polished electrodes benefit from the reduction in surface roughness leading to uniform surface conductivity and the other factors (presence of oxygenous groups on the surface, sp^2 carbon content, boron doping level) have minor effect when considering electrochemical behaviour of these redox markers.

Additionally, EIS measurements were performed in 0.1 mol L^{-1} KCl at 0 V to evaluate the effect of boron content and CM polishing on capacitance values. Nyquist plots in the frequency range from 100 000 Hz to 0.1 Hz in 1 M KCl are shown in Fig. S9 (with a detail for 100 kHz to 10 Hz in Fig. S10). Data were fitted by the equivalent circuit containing constant phase element (CPE) which is depicted in Fig. S10a). The obtained values of parameter Y_0 (characterizing capacitance of the double layer) and N parameter (characterizing the extent of difference in roughness of the surface) are listed in Tab. 3. Y_0 values increase with increasing boron content reaching values from 4500 nMho $s^{-1}cm^{-2}$ to 13000 nMho $s^{-1}cm^{-2}$ for as-grown BDD_{500} to BDD_{8000} films and from 12000 nMho $s^{-1}cm^{-2}$ to 40000 nMho $s^{-1}cm^{-2}$ for CM polished BDD_{500} to BDD_{8000} films, respecting the increasing number of charge transfer carriers with increasing boron doping level known from other EIS studies on BDD electrodes [48,49,55]. Much higher Y^0 values are observed on the CM polished in comparison with as-grown BDD due to the contribution of a higher number of boron-rich places in BDD films and the uniformity of surface morphology after CM polishing. The increased Y^0 value for CM polished BDD_{1000} electrode documents the presence of residual structure features (Tab. 3) in comparison with another CM polished BDD electrodes. The N values are getting smaller with increasing boron content in the BDD electrodes. This trend is nicely seen in the Fig. S10 of the EIS measurements of KCl where with smaller N values the fitted curve is getting closer to the *x* axis which indicates increasing deviation from the ideal capacitance.

Nyquist plots obtained from EIS measurements of 1 mmol L^{-1} $[Fe(CN)_6]^{3-/4-}$ in 1 mol L^{-1} KCl at a potential of $+E = 0.25$ V are depicted in Fig. S11. The R_{ct} values obtained from fitted circuit (inset in Fig. S11a) are listed in Tab. 3. Obviously, they match with data obtained from cyclic voltammetry. With higher boron content the redox process on BDD electrodes runs easier with regards to the R_{ct} and, obviously, the charge transfer resistances are much lower on the CM polished BDD electrodes in comparison with as-grown BDD electrodes. Again, EIS results demonstrate the superiority of surfaces treated by chem-mechanical polishing in comparison with those without it.

A thorough comparison with as-grown and CM polished electrodes studied in this work with other BDD electrodes can be performed based on the overview of electrochemical parameters in Tab. S3. BDD electrodes with metallic-type conductivity (*i.e.*, [B] > 2 × 10^{20} cm^{-3} [11]) exhibit in general lower ΔE_p values for $[Ru(NH_3)_6]^{3+/2+}$ than for $[Fe(CN)_6]^{3-/4-}$ in concordance with our study and with the outer sphere character of the former redox probe. The other trend which can be seen are higher ΔE_p values for $[Fe(CN)_6]^{3-/4-}$ on O-terminated in comparison with H-terminated surface. However, the extent of hydrogenation/oxidation of the surface is usually not supported by XPS or other data and only the method used for surface treatment is described, which makes comparison of ΔE_p values problematic. ΔE_p values for $[Fe(CN)_6]^{3-/4-}$ obtained in our study on CM polished electrodes in the range from 75 mV to 100 mV are close to 65 mV obtained for BDD alumina polished surface with [B] ≈ 1.9 × 10^{20} cm^{-3} [12] or 114 mV for frequently used commercial BDD electrode (B/C 1000 ppm, formerly Windsor Scientific (UK), now Biologic SAS (France)) [26]. C_{dl} values estimated for various BDD electrodes in Tab. S3 can be compared with Y_0 values characterizing the capacitance obtained in our study. Values of C_{dl}< 17.3 μF cm^{-2} characterize the capacitance of BDD electrodes overviewed in Tab. S3, and are comparable with Y_0 values for the as-grown set. Higher values of Y_0 for CM polished samples are presumably caused by uniform conductivity of the surface due to smoothing of the surface following CM polishing. Values are close to those obtained on uniform sp^2 carbon surfaces.

3.5. Electrochemical study of dopamine

To further probe and compare the electrochemical performance of as-grown and CM polished BDD electrodes, voltammetric experiments were performed with a more complex organic redox couple structure, dopamine/dopamine-*o*-quinone, in 0.1 mol L^{-1} phosphate buffer pH 7.4. Dopamine was selected as its redox reaction is well-defined (in pH ~ 7 involves exchange of 2 H^+ and 2 e^- [56]; dopamine is positively charged at this pH (pK_a = 8.93) [57]**.** It proceeds through inner-sphere electron transfer, which makes dopamine very sensitive to the surface and electronic characteristics of the BDD electrodes. This sensitivity can be clearly recognized by differences of ΔE_p values due to changes of HET kinetics for the quasireversible dopamine redox system, being dependent on surface termination [20,49,58–60], sp^2 carbon impurities [20,61], and boron content [48].

3.5.1 Cyclic voltammetry

Cyclic voltammograms recorded in dopamine solution (1 mmol L^{-1}) in the potential range from −0.5 V to +1.5 V on all studied electrodes are depicted in Fig. 7 and valuable parameters extracted from these measurements are summarized in Tab. 4.

On as-grown BDD electrodes, a trend in the shift of the anodic peak potential (E_{pA}), corresponding to dopamine oxidation, toward lower potential values with increasing boron doping can be clearly identified (Fig. 7a); specifically, a dramatic difference of ~430 mV was recognized in E_{pA} between as-grown BDD_{500} and BDD_{8000} electrodes. In addition, only on electrodes prepared at higher B/C, *i.e.*, BDD_{4000} and BDD_{8000}, a small cathodic peak, ascribed to reduction of dopamine-*o*-quinone back to dopamine, was recognized at a potential of ~0 V (see inset in Fig. 7a). Hence, dopamine redox reaction exhibits the fully irreversible nature on as-grown BDD electrodes deposited at lower B/C (≤ 2000 ppm). As can be further seen in Fig. 7a, the intensity of oxidation peak current (I_{pA}) gradually increased with an increase in B/C and the I_{pA} recorded on as-grown BDD_{8000} almost doubled, compared to BDD_{500}. The observed phenomena can be ascribed to the higher doping levels and thus higher conductivity facilitating dopamine/dopamine-*o*-quinone redox reactions [48], but also to the presence of sp^2 carbon impurities, whose increased content was confirmed in as-grown BDD_{4000} and BDD_{8000} by Raman spectroscopy (see Fig. S2). The impact of sp^2-bonded carbon presumably results from the synergic effect of its electrocatalytic and adsorption-promoting role, while the latter may cause, to some extent, 'preconcentration' of dopamine molecules or oxidation product(s) on the BDD surface [20,48].

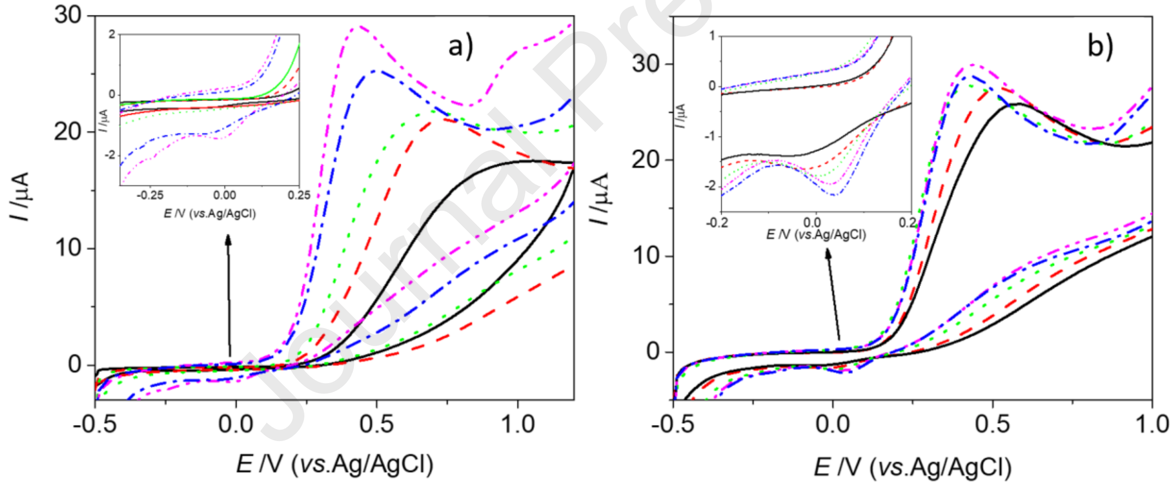

Fig. 7. CVs of 1 mmol L^{-1} dopamine in 0.1 mol L^{-1} phosphate buffer pH 7.4 recorded on (**A**) as-grown BDD and (**B**) CM polished BDD electrodes: (—) BDD_{500}, (– –) BDD_{1000}, (• • •) BDD_{2000}, (– • –) BDD_{4000}, and (– • •) BDD_{8000}, using a scan rate of 0.1 V s^{-1}.

Similar trends, *i.e.*, a decrease in E_{pA} along with an increase in I_{pA} with boron content was observed on CM polished BDD electrodes (see Fig. 7b), however, both trends were significantly less pronounced in comparison with as-grown electrodes. Specifically, (i) a shift in E_{pA} occurred within a much narrower potential range (from +558 mV to +408 mV) and E_{pA} even remained constant for electrodes with B/C ≥ 2000 ppm, and (ii) a difference in the I_{pA} intensity of only ~17 % between CM polished BDD_{500} and BDD_{8000} was discerned. In contrast to as-grown electrodes, a cathodic peak is clearly developed on all CM polished BDD electrodes, as shown in the inset in Fig. 7b, indicating the increased reversible behaviour of the dopamine/dopamine-o-quinone redox system. Importantly, parameters characterizing 'reversibility', ΔE_p and $|I_{pA}/I_{pC}|$ ratio (Tab. 4), improved with increased doping levels. Lower ΔE_p values, and thus faster HET kinetics, were recognized on CM polished BDD of higher B/C ≥ 2000 ppm which is related to the greater content of electroactive sites, *i.e.*, boron atoms and sp^2 carbon spots, accelerating dopamine redox reaction. It has been previously postulated that the more sp^2 carbon present on the BDD surface, the larger the dopamine adsorption is, which consequently manifests in a smaller ΔE_p [61]. Obviously HET kinetics of dopamine is more sensitive to boron doping level and sp^2 carbon content being accelerated with their increase, than HET kinetics of $Fe(CN)_6]^{3-/4-}$. Naturally, HET kinetics benefits from the uniformity of the CM polished surfaces as confirmed for the other redox markers.

Finally, as can be seen in Tab. 4, the differences between as-grown and CM polished electrodes are more evident at lower B/C, while with an increase in the content of boron dopant and sp^2 carbon sites, differences gradually diminish resulting in much more comparable dopamine responses, most visibly on BDD_{8000}, regardless of the surface microstructure (as-grown *vs.* CM polished).

Tab. 4: Parameters extracted from CVs recorded on as-grown and CM polished BDD electrodes characterizing dopamine/dopamine-o-quinone redox reaction: dopamine oxidation potential (E_{pA}), the peak-to-peak separation (ΔE_p), and the ratio of anodic and cathodic peak currents $|I_{pA}/I_{pC}|$.

	as-grown	CM polished	as-grown	CM polished	as-grown	CM polished
Sample	E_{pA} (mV)		ΔE_p (mV)		$\lvert I_{pA}/I_{pC}\rvert$	
BDD_{500}	+840	+558	[a]–	501	[a]–	18.5
BDD_{1000}	+699	+480	[a]–	423	[a]–	16.8
BDD_{2000}	+537	+410	[a]–	353	[a]–	15.4
BDD_{4000}	+459	+408	447	351	19.4	14.9
BDD_{8000}	+414	+408	384	351	20.2	13.7

[a]Values are not reported, as cathodic peak is absent in the recorded CVs.

3.5.2 Square-wave voltammetry

Clearly, CV experiments revealed the enhanced electrochemical performance of CM polished BDD electrodes. To verify that such a significant boost also translates into improved analytical parameters essential for the development of electrochemical sensors, further voltammetric experiments were performed with as-grown and CM polished BDD_{500} and BDD_{4000} electrodes. These four electrodes were selected to act as representatives of electrodes with lower and higher boron and sp^2 carbon content, and simultaneously they reflect either more or less pronounced differences among the two sets. Specifically, a well-established, and sensitive SWV technique with previously optimized parameters (overviewed in Section 2.3 for each electrode) was employed to record concentration dependences of dopamine (Fig. S12). The obtained analytical parameters, *i.e.*, linear dynamic range (LDR) and calculated *LOD* values, using the procedure described in Section 2.3, for all four BDD electrodes are reported in Tab. 5.

The widest LDR providing linear current responses for the entire range of dopamine concentrations (from 1.0 to 100.0 μmol L^{-1}) was only obtained on the CM polished BDD_{4000} electrode, whereas a break in the linear range occurred on the other three studied electrodes (see Fig. S12). Similarly, two LDR within the investigated concentration range have been recognized in previous studies on catecholamine neurotransmitters, dopamine [49,62] and epinephrine [63], and their metabolite vanillylmandelic acid [64]. Further, assessing both sets individually, higher doped BDD_{4000} electrodes provided lower *LOD* values, compared to BDD_{500} electrodes. Nevertheless, when the two sets are compared, CM polished electrodes certainly outperform both as-grown BDD electrodes, *i.e.*, even CM polished BDD_{500} exhibits better electroanalytical characteristics than as-grown BDD_{4000} (see Table 4). Overall, the lowest *LOD* of 0.23 μmol L^{-1} and the highest sensitivity was achieved on CM polished BDD_{4000}. Apparently, smoother surfaces with larger areas of exposed and thus available electroactive sites including boron atoms and sp^2 carbon domains, whose effects were thoroughly discussed above, contribute to the superior electroanalytical performance of CM polished BDD electrodes. The achieved submicromolar *LOD*s and *LDR* over two orders of magnitude for the CM polished BDD_{4000} electrode is comparable with analytical figures of merit obtained on other non-modified O- and H-terminated BDD electrodes as can be seen from the overview of their analytical performance in Tab. S4.

Tab. 5: Analytical parameters of concentration dependences of dopamine in 0.1 mol L^{-1} phosphate buffer of pH 7.4 obtained by SWV using optimized parameters, with calculated *LOD* values.

BDD electrode	LDR (µmol L^{-1})	Slope (nA µmol L^{-1})	Intercept (nmol L^{-1})	*R*	*LOD* (µmol L^{-1})
As-grown					
BDD_{500}	6.0 – 20.0	4.9 ± 0.4	−0.020 ± 0.003	0.9899	1.82
	20.0 – 100.0	11.8 ± 0.7	−0.133 ± 0.032	0.9931	
BDD_{4000}	2.0 – 10.0	3.7 ± 0.2	−0.004 ± 0.001	0.9940	1.06
	10.0 – 80.0	6.8 ± 0.2	−0.044 ± 0.006	0.9984	
CM polished					
BDD_{500}	4.0 – 10.0	3.6 ± 0.2	−0.008 ± 0.001	0.9964	0.84
	10.0 – 80.0	11.2 ± 0.4	−0.086 ± 0.006	0.9976	
BDD_{4000}	1.0 – 100.0	52.6 ± 1.1	−0.020 ± 0.004	0.9987	0.23

4. Conclusion

A thorough experimental study was performed with a set of ultra-thin (≤ 500 nm) BDD layers deposited at B/C ratios 500 ppm – 8000 ppm aiming at comparison of as-grown polycrystalline and CM polished electrodes.

The main effects of the CM polishing can be summarized as follows:

(i) The CM polished electrode (BDD_{2000}) exhibits a strong texture with component in the {011} and {111} orientation, confirmed by EBSD measurements.

(ii) Raman spectroscopy revealed an increase in sp^2 carbon content in BDD_{4000} and BDD_{8000} electrodes in comparison with lower doped $BDD_{500\text{-}2000}$ electrodes, and importantly, CM polishing did not cause any increase in amount of sp^2 carbon impurities (regarding sensitivity of Raman measurements).

(iii) XPS revealed the higher surface quality of CM polished BDD layers, only a minor rise in oxygen content and an increase in boron content for BDD_{4000} and BDD_{8000} electrodes in comparison with as-grown layers. This effect can be explained by CM polishing exposing boron atoms present in bulk of the BDD, where the concentration is higher than on the surface due to a "shut-down" effect during the switch off procedure following CVD leading to diamond deposition with lower [B] content due to changes in the final deposition conditions.

(iv) SECM using FcMeOH as a redox probe proved that the conductivity of as-grown BDD layers is heterogeneously distributed, as-grown surfaces possess spots of high electrochemical activity as well as insulating spots (the latter increases with decreasing boron content). CM polished BDD electrodes exhibit better uniform distribution of surface activity, especially for highly doped BDD, in agreement with uniform distribution of boron atoms in the bulk of BDD layers [43–45].

(v) The increase in Y_0 values characterizing the capacitance with increasing boron content estimated by EIS is presumably caused by an increasing number of charge carriers, represented by boron atoms and sp^2 carbon in BDD_{4000} and BDD_{8000} layers. The higher values of Y_0 and lower values of charge transfer resistance R_{ct} of CM polished in comparison with as-grown layers can be assigned to increased surface boron concentration in BDD_{4000} and BDD_{8000} layers, confirmed by XPS and uniform conductivity of the surface due to smoothing of the surface imposed by polishing.

(vi) The HET kinetics of outer-sphere redox markers ($[IrCl_6]^{2-/3-}$ and $[Ru(NH_3)_6]^{3+/2+}$) sphere is (nearly) reversible, independent on boron doping level and surface morphology. The HET kinetics of inner-sphere redox markers ($[Fe(CN)_6]^{3-/4-}$, dopamine/dopamine-*o*-quinone) is accelerating with increasing boron doping level, as recognized by decreased ΔE_p values. A significant enhancement of HET kinetics (more pronounced for lowly doped films) has been recognized on CM polished BDD electrodes. For $Fe(CN)_6]^{3-/4-}$, the slightly higher amount of oxygenous groups on the CM polished surface, sp^2 carbon content, and boron doping level have minor effect and the HET kinetics accelerates due to reduction in surface roughness leading to uniform surface conductivity. The HET kinetics of dopamine is more sensitive to boron doping level and sp^2 carbon content being accelerated with their increase.

(vii) Electroanalytical characteristics estimated for dopamine in phosphate buffer revealed that BDD_{500} and BDD_{4000} CM polished electrodes outperform BDD_{500} and BDD_{4000} as-grown BDD electrodes. The lowest *LOD* of 0.23 µmol L^{-1}, the widest linear dynamic range and the highest sensitivity was achieved on CM polished BDD_{4000} electrodes.

Obviously, the changes in electrochemical characteristics described in (iv) – (vii) reveal that CM polished BDD electrodes possess uniform distribution of conductivity due to smoothing of the surface as proved by scanning electrochemical microscopy**,** faster heterogenous electron transfer kinetics for inner-sphere redox markers **(**$[Fe(CN)_6]^{3-/4-}$ and dopamine) and higher values of double layer capacitance. However, CM polished surfaces presumably contain uniformly distributed charge carriers as a result of continuous BDD growth during unaltered CVD process, moreover on a relatively smooth surface with less grain boundary influence. This homogeneity of CM polished surfaces is obviously the key parameter for boosting of electrochemical and electroanalytical characteristics. The other major effect influencing electrochemical properties includes increased number of charge carriers, represented by boron atoms, and eventually sp^2 carbon in BDD_{4000} and BDD_{8000} films.

To conclude, CM polishing or other advanced diamond polishing methods [32] seem to be a very effective way for altering the electrochemical properties of BDD. Further studies are needed to evaluate their fouling resistivity, efficacy in productivity of hydroxyl radicals, possibilities of local surface structuring and surface termination to extend their possibilities in (bio)sensing, incineration of organic compounds and electrocatalytic applications.

Acknowledgements

The Czech Science Foundation [project 20-03187S] and Czech Ministry of Education, Youth and Sports projects SOLID21 CZ.02.1.01/0.0/0.0/16_019/0000760 and CzechNanoLab Research Infrastructure LM2018110 and Specific University Research of Charles University [SVV 260560] are gratefully acknowledged.

References

[1] K. Muzyka, J. Sun, T.H. Fereja, Y. Lan, W. Zhang, G. Xu, Boron-doped diamond: current progress and challenges in view of electroanalytical applications, Anal. Methods. 11 (2019) 397–414. https://doi.org/10.1039/C8AY02197J.

[2] B.C. Lourencao, R.F. Brocenschi, R.A. Medeiros, O. Fatibello-Filho, R.C. Rocha-Filho, Analytical Applications of Electrochemically Pretreated Boron-Doped Diamond Electrodes, ChemElectroChem. 7 (2020) 1291–1311. https://doi.org/10.1002/celc.202000050.

[3] N. Yang, S. Yu, J.V. Macpherson, Y. Einaga, H. Zhao, G. Zhao, G.M. Swain, X. Jiang, Conductive diamond: synthesis, properties, and electrochemical applications, Chem. Soc. Rev. 48 (2019) 157–204. https://doi.org/10.1039/C7CS00757D.

[4] S. Baluchová, A. Daňhel, H. Dejmková, V. Ostatná, M. Fojta, K. Schwarzová-Pecková, Recent progress in the applications of boron doped diamond electrodes in electroanalysis of organic compounds and biomolecules – A review, Anal. Chim. Acta. 1077 (2019) 30–66. https://doi.org/10.1016/j.aca.2019.05.041.

[5] R.F. Brocenschi, P. Hammer, C. Deslouis, R.C. Rocha-Filho, Assessments of the Effect of Increasingly Severe Cathodic Pretreatments on the Electrochemical Activity of Polycrystalline Boron-Doped Diamond Electrodes, Anal. Chem. 88 (2016) 5363–5368. https://doi.org/10.1021/acs.analchem.6b00676.

[6] J.V. Macpherson, A practical guide to using boron doped diamond in electrochemical research, Phys. Chem. Chem. Phys. 17 (2015) 2935–2949. https://doi.org/10.1039/C4CP04022H.

[7] S. Garcia-Segura, E. Vieira dos Santos, C.A. Martínez-Huitle, Role of sp3/sp2 ratio on the electrocatalytic properties of boron-doped diamond electrodes: A mini review, Electrochem. Commun. 59 (2015) 52–55. https://doi.org/10.1016/j.elecom.2015.07.002.

[8] Y. Einaga, J.S. Foord, G.M. Swain, Diamond electrodes: Diversity and maturity, MRS Bull. 39 (2014) 525–532. https://doi.org/10.1557/mrs.2014.94.

[9] J. Ryl, A. Zielinski, L. Burczyk, R. Bogdanowicz, T. Ossowski, K. Darowicki, Chemical-Assisted Mechanical Lapping of Thin Boron-Doped Diamond Films: A Fast Route Toward High Electrochemical Performance for Sensing Devices, Electrochimica Acta. 242 (2017) 268–279. https://doi.org/10.1016/j.electacta.2017.05.027.

[10] M. Bernard, C. Baron, A. Deneuville, About the origin of the low wave number structures of the Raman spectra of heavily boron doped diamond films, Diam. Relat. Mater. 13 (2004) 896–899. https://doi.org/10.1016/j.diamond.2003.11.082.

[11] K. Schwarzová-Pecková, J. Vosáhlová, J. Barek, I. Šloufová, E. Pavlova, V. Petrák, J. Zavázalová, Influence of boron content on the morphological, spectral, and electroanalytical characteristics of anodically oxidized boron-doped diamond electrodes, Electrochimica Acta. 243 (2017) 170–182. https://doi.org/10.1016/j.electacta.2017.05.006.

[12] L.A. Hutton, J.G. Iacobini, E. Bitziou, R.B. Channon, M.E. Newton, J.V. Macpherson, Examination of the factors affecting the electrochemical performance of oxygen-terminated polycrystalline boron-doped diamond electrodes, Anal. Chem. 85 (2013) 7230–7240. https://doi.org/10.1021/ac401042t.

[13] A.W.S. Williams, E.C. Lightowlers, A.T. Collins, Impurity conduction in synthetic semiconducting diamond, J. Phys. C Solid State Phys. 3 (1970) 1727–1735. https://doi.org/10.1088/0022-3719/3/8/011.

[14] R. Šelešovská, B. Kränková, M. Štěpánková, P. Martinková, L. Janíková, J. Chýlková, M. Vojs, Influence of boron content on electrochemical properties of boron-doped diamond electrodes and their utilization for leucovorin determination, J. Electroanal. Chem. 821 (2018) 2–9. https://doi.org/10.1016/j.jelechem.2018.02.007.

[15] A.N. Ndao, F. Zenia, A. Deneuville, M. Bernard, C. Lévy-Clément, Effect of boron concentration on the electrochemical reduction of nitrates on polycrystalline diamond electrodes, Diam. Relat. Mater. 9 (2000) 1175–1180. https://doi.org/10.1016/S0925-9635(99)00328-3.

[16] Y. Feng, J. Lv, J. Liu, N. Gao, H. Peng, Y. Chen, Influence of boron concentration on growth characteristic and electro-catalytic performance of boron-doped diamond electrodes prepared by direct current plasma chemical vapor deposition, Appl. Surf. Sci. 257 (2011) 3433–3439. https://doi.org/10.1016/j.apsusc.2010.11.041.
[17] J. Li, C.L. Bentley, S. Tan, V.S.S. Mosali, M.A. Rahman, S.J. Cobb, S.-X. Guo, J.V. Macpherson, P.R. Unwin, A.M. Bond, J. Zhang, Impact of sp^2 Carbon Edge Effects on the Electron-Transfer Kinetics of the Ferrocene/Ferricenium Process at a Boron-Doped Diamond Electrode in an Ionic Liquid, J. Phys. Chem. C. 123 (2019) 17397–17406. https://doi.org/10.1021/acs.jpcc.9b04519.
[18] J.A. Bennett, J. Wang, Y. Show, G.M. Swain, Effect of sp2-Bonded Nondiamond Carbon Impurity on the Response of Boron-Doped Polycrystalline Diamond Thin-Film Electrodes, J. Electrochem. Soc. (n.d.) 9.
[19] I. Duo, A. Fujishima, C. Comninellis, Electron transfer kinetics on composite diamond (sp3)–graphite (sp2) electrodes, Electrochem. Commun. 5 (2003) 695–700. https://doi.org/10.1016/S1388-2481(03)00169-3.
[20] T. Watanabe, Y. Honda, K. Kanda, Y. Einaga, Tailored design of boron-doped diamond electrodes for various electrochemical applications with boron-doping level and sp^2 -bonded carbon impurities: Tailored design of boron-doped diamond electrodes, Phys. Status Solidi A. 211 (2014) 2709–2717. https://doi.org/10.1002/pssa.201431455.
[21] S.C. B. Oliveira, A.M. Oliveira-Brett, Voltammetric and electrochemical impedance spectroscopy characterization of a cathodic and anodic pre-treated boron doped diamond electrode, Electrochimica Acta. 55 (2010) 4599–4605. https://doi.org/10.1016/j.electacta.2010.03.016.
[22] V. Rehacek, I. Hotovy, M. Marton, M. Mikolasek, P. Michniak, A. Vincze, A. Kromka, M. Vojs, Voltammetric characterization of boron-doped diamond electrodes for electroanalytical applications, J. Electroanal. Chem. 862 (2020) 114020. https://doi.org/10.1016/j.jelechem.2020.114020.
[23] H.B. Suffredini, V.A. Pedrosa, L. Codognoto, S.A.S. Machado, R.C. Rocha-Filho, L.A. Avaca, Enhanced electrochemical response of boron-doped diamond electrodes brought on by a cathodic surface pre-treatment, Electrochimica Acta. 49 (2004) 4021–4026. https://doi.org/10.1016/j.electacta.2004.01.082.
[24] Z.V. Živcová, V. Petrák, O. Frank, L. Kavan, Electrochemical impedance spectroscopy of polycrystalline boron doped diamond layers with hydrogen and oxygen terminated surface, Diam. Relat. Mater. 55 (2015) 70–76. https://doi.org/10.1016/j.diamond.2015.03.002.
[25] F. Marken, C.A. Paddon, D. Asogan, Direct cytochrome c electrochemistry at boron-doped diamond electrodes, Electrochem. Commun. 4 (2002) 62–66. https://doi.org/10.1016/S1388-2481(01)00272-7.
[26] J. Zavazalova, K. Prochazkova, K. Schwarzova-Peckova, Boron-doped Diamond Electrodes for Voltammetric Determination of Benzophenone-3, Anal. Lett. 49 (2016) 80–91. https://doi.org/10.1080/00032719.2014.1003425.
[27] J. Klouda, K. Nesměrák, P. Kočovský, J. Barek, K. Schwarzová-Pecková, A novel voltammetric approach to the detection of primary bile acids in serum samples, Bioelectrochemistry Amst. Neth. 134 (2020) 107539. https://doi.org/10.1016/j.bioelechem.2020.107539.
[28] E.L.H. Thomas, G.W. Nelson, S. Mandal, J.S. Foord, O.A. Williams, Chemical mechanical polishing of thin film diamond, Carbon. 68 (2014) 473–479. https://doi.org/10.1016/j.carbon.2013.11.023.
[29] E.L.H. Thomas, S. Mandal, E.B. Brousseau, O.A. Williams, Silica based polishing of 100 and 111 single crystal diamond, Sci. Technol. Adv. Mater. 15 (2014) 035013. https://doi.org/10.1088/1468-6996/15/3/035013.
[30] A. Peguiron, G. Moras, M. Walter, H. Uetsuka, L. Pastewka, M. Moseler, Activation and mechanochemical breaking of C–C bonds initiate wear of diamond (110) surfaces in contact with silica, Carbon. 98 (2016) 474–483. https://doi.org/10.1016/j.carbon.2015.10.098.

[31] G.M. Klemencic, S. Mandal, J.M. Werrell, S.R. Giblin, O.A. Williams, Superconductivity in planarised nanocrystalline diamond films, Sci. Technol. Adv. Mater. 18 (2017) 239–244. https://doi.org/10.1080/14686996.2017.1286223.
[32] C. Xiao, F.-C. Hsia, A. Sutton-Cook, B. Weber, S. Franklin, Polishing of polycrystalline diamond using synergies between chemical and mechanical inputs: A review of mechanisms and processes (in press), Carbon 196 (2022) 29–48. https://doi.org/10.1016/j.carbon.2022.04.028.
[33] F. Silva, A. Gicquel, A. Tardieu, P. Cledat, Th. Chauveau, Control of an MPACVD reactor for polycrystalline textured diamond films synthesis: role of microwave power density, Diam. Relat. Mater. 5 (1996) 338–344. https://doi.org/10.1016/0925-9635(95)00428-9.
[34] C. Wei, A.J. Bard, M.V. Mirkin, Scanning Electrochemical Microscopy. 31. Application of SECM to the Study of Charge Transfer Processes at the Liquid/Liquid Interface, J. Phys. Chem. 99 (1995) 16033–16042. https://doi.org/10.1021/j100043a050.
[35] Y. Wang, J. Lin, R. Zong, J. He, Y. Zhu, Enhanced photoelectric catalytic degradation of methylene blue via TiO2 nanotube arrays hybridized with graphite-like carbon, J. Mol. Catal. Chem. 349 (2011) 13–19. https://doi.org/10.1016/j.molcata.2011.08.020.
[36] R.S. Nicholson, Theory and Application of Cyclic Voltammetry for Measurement of Electrode Reaction Kinetics., Anal. Chem. 37 (1965) 1351–1355. https://doi.org/10.1021/ac60230a016.
[37] A.J. Bard, L.R. Faulkner, Electrochemical methods: fundamentals and applications, 2nd ed, Wiley, New York, 2001.
[38] J.J. Watkins, H.S. White, The Role of the Electrical Double Layer and Ion Pairing on the Electrochemical Oxidation of Hexachloroiridate(III) at Pt Electrodes of Nanometer Dimensions, Langmuir. 20 (2004) 5474–5483. https://doi.org/10.1021/la0496993.
[39] J.A.N. Gonçalves, G.M. Sandonato, K. Iha, Characterization of boron doped CVD diamond films by Raman spectroscopy and X-ray diffractometry, Diam. Relat. Mater. 11 (2002) 1578–1583. https://doi.org/10.1016/S0925-9635(02)00103-6.
[40] V. Mortet, Z.V. Živcová, A. Taylor, M. Davydová, O. Frank, P. Hubík, J. Lorincik, M. Aleshin, Determination of atomic boron concentration in heavily boron-doped diamond by Raman spectroscopy, Diam. Relat. Mater. 93 (2019) 54–58. https://doi.org/10.1016/j.diamond.2019.01.028.
[41] V. Mortet, Z. Vlčková Živcová, A. Taylor, O. Frank, P. Hubík, D. Trémouilles, F. Jomard, J. Barjon, L. Kavan, Insight into boron-doped diamond Raman spectra characteristic features, Carbo. 115 (2017) 279–284. https://doi.org/10.1016/j.carbon.2017.01.022.
[42] S. Ferro, M. Dal Colle, A. De Battisti, Chemical surface characterization of electrochemically and thermally oxidized boron-doped diamond film electrodes, Carbon 43 (2005) 1191–1203. https://doi.org/10.1016/j.carbon.2004.12.012.
[43] F. Jia, Y. Bai, F. Qu, J. Zhao, C. Zhuang, X. Jiang, Effect of B/C ratio on the physical properties of highly boron-doped diamond films, Vacuum. 84 (2010) 930–934. https://doi.org/10.1016/j.vacuum.2010.01.003.
[44] A.F. Azevedo, F.A. Souza, P. Hammer, M.R. Baldan, N.G. Ferreira, The influence of hydrogen plasma pre-treatment on the structure of BDND electrode surface applied for phenol detection, J. Nanoparticle Res. 13 (2011) 6133–6139. https://doi.org/10.1007/s11051-011-0501-1.
[45] P. Ashcheulov, A. Taylor, Z. Vlčková Živcová, P. Hubík, J. Honolka, M. Vondráček, M. Remzová, J. Kopeček, L. Klimša, J. Lorinčik, M. Davydova, Z. Remeš, M. Kohout, A.M. Beltran, V. Mortet, Low temperature synthesis of transparent conductive boron doped diamond films for optoelectronic applications: Role of hydrogen on the electrical properties, Appl. Mater. Today. 19 (2020) 100633. https://doi.org/10.1016/j.apmt.2020.100633.
[46] J.I.B. Wilson, J.S. Walton, G. Beamson, Analysis of chemical vapour deposited diamond films by X-ray photoelectron spectroscopy, J. Electron Spectrosc. Relat. Phenom. 121 (2001) 183–201. https://doi.org/10.1016/S0368-2048(01)00334-6.
[47] P. Kuang, K. Natsui, C. Feng, Y. Einaga, Electrochemical reduction of nitrate on boron-doped diamond electrodes: Effects of surface termination and boron-doping level, Chemosphere. 251 (2020) 126364. https://doi.org/10.1016/j.chemosphere.2020.126364.

[48] S. Baluchová, A. Taylor, V. Mortet, S. Sedláková, L. Klimša, J. Kopeček, O. Hák, K. Schwarzová-Pecková, Porous boron doped diamond for dopamine sensing: Effect of boron doping level on morphology and electrochemical performance, Electrochimica Acta. 327 (2019) 135025. https://doi.org/10.1016/j.electacta.2019.135025.

[49] M. Brycht, S. Baluchová, A. Taylor, V. Mortet, S. Sedláková, L. Klimša, J. Kopeček, K. Schwarzová-Pecková, Comparison of electrochemical performance of various boron-doped diamond electrodes: Dopamine sensing in biomimicking media used for cell cultivation, Bioelectrochemistry. 137 (2021) 107646. https://doi.org/10.1016/j.bioelechem.2020.107646.

[50] S. Sainio, T. Palomäki, S. Rhode, M. Kauppila, O. Pitkänen, T. Selkälä, G. Toth, M. Moram, K. Kordas, J. Koskinen, T. Laurila, Carbon nanotube (CNT) forest grown on diamond-like carbon (DLC) thin films significantly improves electrochemical sensitivity and selectivity towards dopamine, Sens. Actuators B Chem. 211 (2015) 177–186. https://doi.org/10.1016/j.snb.2015.01.059.

[51] G.P. Keeley, M.E.G. Lyons, The effects of thin layer diffusion at glassy carbon electrodes modified with porous films of single-walled carbon nanotubes, Int. J. Electrochem. Sci. 4 (2009) 794–809.

[52] I. Streeter, G.G. Wildgoose, L. Shao, R.G. Compton, Cyclic voltammetry on electrode surfaces covered with porous layers: An analysis of electron transfer kinetics at single-walled carbon nanotube modified electrodes, Sens. Actuators B Chem. 133 (2008) 462–466. https://doi.org/10.1016/j.snb.2008.03.015.

[53] R.L. McCreery, Advanced Carbon Electrode Materials for Molecular Electrochemistry, Chem. Rev. 108 (2008) 2646–2687. https://doi.org/10.1021/cr068076m.

[54] K.B. Holt, A.J. Bard, Y. Show, G.M. Swain, Scanning Electrochemical Microscopy and Conductive Probe Atomic Force Microscopy Studies of Hydrogen-Terminated Boron-Doped Diamond Electrodes with Different Doping Levels, J. Phys. Chem. B. 108 (2004) 15117–15127. https://doi.org/10.1021/jp048222x.

[55] T. Watanabe, T.K. Shimizu, Y. Tateyama, Y. Kim, M. Kawai, Y. Einaga, Giant electric double-layer capacitance of heavily boron-doped diamond electrode, Diam. Relat. Mater. 19 (2010) 772–777. https://doi.org/10.1016/j.diamond.2010.02.022.

[56] A.N. Patel, S. Tan, T.S. Miller, J.V. Macpherson, P.R. Unwin, Comparison and Reappraisal of Carbon Electrodes for the Voltammetric Detection of Dopamine, Anal. Chem. 85 (2013) 11755–11764. https://doi.org/10.1021/ac401969q.

[57] https://pubchem.ncbi.nlm.nih.gov/compound/681 (accessed November 11, 2022).

[58] R. Trouillon, D. O'Hare, Y. Einaga, Effect of the doping level on the biological stability of hydrogenated boron doped diamond electrodes, Phys. Chem. Chem. Phys. 13 (2011) 5422–5429. https://doi.org/10.1039/C0CP02420A.

[59] Z. Liu, S. Baluchová, A.F. Sartori, Z. Li, Y. Gonzalez-Garcia, M. Schreck, J.G. Buijnsters, Heavily boron-doped diamond grown on scalable heteroepitaxial quasi-substrates: A promising single crystal material for electrochemical sensing applications, Carbon. 201 (2023) 1229–1240. https://doi.org/10.1016/j.carbon.2022.10.023.

[60] R. Trouillon, Y. Einaga, M.A.M. Gijs, Cathodic pretreatment improves the resistance of boron-doped diamond electrodes to dopamine fouling, Electrochem. Commun. 47 (2014) 92–95. https://doi.org/10.1016/j.elecom.2014.07.028.

[61] S. Wang, V.M. Swope, J.E. Butler, T. Feygelson, G.M. Swain, The structural and electrochemical properties of boron-doped nanocrystalline diamond thin-film electrodes grown from Ar-rich and H2-rich source gases, Diam. Relat. Mater. 18 (2009) 669–677. https://doi.org/10.1016/j.diamond.2008.11.033.

[62] D.B. Gorle, M.A. Kulandainathan, Electrochemical sensing of dopamine at the surface of a dopamine grafted graphene oxide/poly(methylene blue) composite modified electrode, RSC Adv. 6 (2016) 19982–19991. https://doi.org/10.1039/C5RA25541D.

[63] X. Liu, D. Ye, L. Luo, Y. Ding, Y. Wang, Y. Chu, Highly sensitive determination of epinephrine by a MnO2/Nafion modified glassy carbon electrode, J. Electroanal. Chem. 665 (2012) 1–5. https://doi.org/10.1016/j.jelechem.2011.06.030.

[64] Q. Li, C. Batchelor-McAuley, R.G. Compton, Electrooxidative Decarboxylation of Vanillylmandelic Acid: Voltammetric Differentiation between the Structurally Related Compounds Homovanillic Acid and Vanillylmandelic Acid, J. Phys. Chem. B. 114 (2010) 9713–9719. https://doi.org/10.1021/jp104137p.

- Chem-mechanical polishing of BDD with various [B] content
- Full EBSD characterisation of chem-mechanical polished BDD
- Chem-mechanical polishing reveals bulk [B] content to the surface
- Chem-mechanical polishing leads to uniform distribution of electro-chemical surface activity
- Significant enhancement of HET kinetics recognized on chem-mechanical polished BDD electrodes
- Superior electroanalytical performance of chem-mechanical polished BDD electrodes for dopamine detection

Declaration of interests

☒ The authors declare that they have no known competing financial interests or personal relationships that could have appeared to influence the work reported in this paper.

☐ The authors declare the following financial interests/personal relationships which may be considered as potential competing interests: